Ambiguity Function Shaping for Cognitive Radar Via Complex Quartic Optimization

Augusto Aubry, *Member, IEEE*, Antonio De Maio, *Fellow, IEEE*, Bo Jiang, and Shuzhong Zhang

***Abstract*—In this paper, we propose a cognitive approach to design phase-only modulated waveforms sharing a desired range-Doppler response. The idea is to minimize the average value of the ambiguity function of the transmitted signal over some range-Doppler bins, which are identified exploiting a plurality of knowledge sources. From a technical point of view, this is tantamount to optimizing a real and homogeneous complex quartic order polynomial with a constant modulus constraint on each optimization variable. After proving some interesting properties of the considered problem, we devise a polynomial-time waveform optimization procedure based on the Maximum Block Improvement (MBI) method and the theory of conjugate-partial-symmetric/conjugate-super-symmetric fourth order tensors. At the analysis stage, we assess the performance of the proposed technique showing its capability to properly shape the range-Doppler response of the transmitted waveform.**

***Index Terms*—Cognitive radar, radar waveform optimization, maximum block improvement method, complex tensor optimization.**

I. Introduction

In radar signal processing, a key role is played by the range-Doppler response of the waveform used to probe the environment. In fact, it controls both Doppler and range resolutions of the system; besides, it also regulates the interference power, produced by unwanted returns, at the output of the matched filter to the target signature. In the context of fast-time coding, the aforementioned response is usually referred to as the classic waveform *ambiguity function* [1]–[3] and the problem of designing signals sharing a desired ambiguity [4]–[6] or a given zero-Doppler ambiguity cut (also known as range profile) [7], [8], [9], [10], [11], has attracted the interest of many radar researchers since the early days of radar. If a slow-time coding is considered, then the waveform range-Doppler response can be interpreted as a *slow-time ambiguity function*, namely each cut along a line parallel to the Doppler axis is the Doppler response of the filter (matched to the transmitted waveform) to an echo (arising from a potential useful target and/or an interference return) which is located at a given number of Pulse Repetition Intervals (PRI) away from the one of interest.

In this work, we propose a cognitive approach to devise radar waveforms sharing a desired range-Doppler response. The importance of this study is motivated by the potential of the cognitive paradigm which is becoming one of the leading approaches for advanced signal processing techniques, attempting to satisfy more and more demanding system performance requirements [12], [16].

We suppose that the radar system can exploit a plurality of knowledge sources. Specifically, it can predict the actual scattering environment, using a dynamic environmental database, including a geographic information system, meteorological data, previous scans, and some electromagnetic reflectivity and spectral clutter models. Hence, exploiting the above information, the radar look-ahead coprocessor ([12], p. 27) can locate the range-Doppler bins where strong unwanted returns are foreseen and, consequently, transmit a waveform whose ambiguity function exhibits low values in those interfering bins. This framework is particularly attractive for the confirmation process where a previous detection, performed through a standard radar waveform, can be reliably confirmed using a signal matched to the specific range-Doppler interference scenario.

The adopted design criterion minimizes the average value of the ambiguity function (over the identified range-Doppler bins) with respect to the radar phase-only waveform. Specifically, we formulate the problem as a complex quartic order polynomial optimization problem [13]–[15] with constant modulus constraints forced to ensure phase-only modulated signals, compatible with today amplifier's technology [17], [18]. After proving that the optimization problem falls into an NP-hard class, we propose a new solution technique based on the Maximum Block Improvement (MBI) method, which is an iterative algorithm known to achieve excellent performances in the optimization of real polynomial functions subject to spherical constraints [19]. First we devise three MBI type optimization algorithms, based on a linear- and a quadratic-improvement subroutines; then, we obtain our radar signal as the best solution among them. At the analysis stage, we provide some numerical results showing the effectiveness of the proposed method to provide a radar waveform with a desired range-Doppler behavior.

The paper is organized as follows. In Section II, we describe the system model and formulate the waveform design problem. In Section III, we analyze the properties of the obtained optimization problem and propose a solution technique based on the MBI

Manuscript received January 03, 2013; revised May 18, 2013 and July 05, 2013; accepted July 05, 2013. Date of publication July 18, 2013; date of current version October 11, 2013. The associate editor coordinating the review of this manuscript and approving it for publication was Prof. Maria Sabrina Greco. The work of B. Jiang and S. Zhang was supported in part by National Science Foundation under Grant CMMI-1161242.

A. Aubry is with CNR, IREA, I-80124 Napoli, Italy (e-mail: aubry.a@irea.cnr.it).

A. De Maio is with the Università degli Studi di Napoli "Federico II", Dipartimento di Ingegneria Biomedica Elettronica e delle Telecomunicazioni, I-80125 Napoli, Italy (e-mail: ademaio@unina.it).

B. Jiang and S. Zhang are with the Department of Industrial and Systems Engineering, University of Minnesota, Minneapolis, MN 55455 USA (e-mail: jiang373@umn.edu; zhangs@umn.edu).

Color versions of one or more of the figures in this paper are available online at http://ieeexplore.ieee.org.

Digital Object Identifier 10.1109/TSP.2013.2273885

method and the theory of conjugate-partial-symmetric/conjugate-super-symmetric fourth order tensors. In Section IV, we present the performance of the devised algorithm. Finally, in Section V, we draw conclusions and outline some possible future research tracks.

A. Notation

We adopt the notation of using boldface for vectors $\boldsymbol{a}$ (lower case), and matrices $\boldsymbol{A}$ (upper case), while tensors are indicated with calligraphic upper case letter $\mathcal{F}$. The transpose, the conjugate, and the conjugate transpose operators are denoted by the symbols $(\cdot)^T$, $\bar{(\cdot)}$, and $(\cdot)^\dagger$ respectively. $\boldsymbol{I}$ denotes the identity matrix (its size is determined from the context). $\mathbb{R}^N$, $\mathbb{C}^N$, $\mathbb{C}^{N,N}$, and $\mathbb{C}^{N,N,N,N}$ are respectively the set of N-dimensional vectors of real numbers, the set of N-dimensional vectors of complex numbers, the set of $N \times N$ matrices of complex numbers, and the set of $N \times N \times N \times N$ fourth order tensors of complex numbers. The Euclidean norm of the vector $\boldsymbol{x}$ is denoted by $\|\boldsymbol{x}\|$. The letter j represents the imaginary unit (i.e., $j = \sqrt{-1}$), while the letter i often serves as index in this paper. For any complex number x, we use $\Re(x)$ and $\Im(x)$ to denote respectively the real and the imaginary part of x; also, $|x|$ and $\arg(x)$ represent the modulus and the argument of x. For any finite set A, $Card(A)$ indicates the cardinality of the set A. $\mathbb{E}[\cdot]$ denotes statistical expectation. Finally, $\odot$ denotes the Hadamard product and for any optimization problem P, $v(\mathrm{P})$ represents its optimal value.

II. System Model & Problem Formulation

We consider a monostatic radar system which transmits a coherent burst of N slow-time coded pulses. Let us denote by $\boldsymbol{s} = [s(1), \ldots, s(N)]^T \in \mathbb{C}^N$ the radar code. The waveform at the receiver end is down-converted to baseband, undergoes a pulse matched filtering operation, and then is sampled. The N-dimensional column vector $\boldsymbol{v} = [v(1), \ldots, v(N)]^T \in \mathbb{C}^N$ of the observations, from the range-azimuth cell under test, can be expressed as:

$$\boldsymbol{v} = \alpha_T \boldsymbol{s} \odot \boldsymbol{p}(\nu_{d_T}) + \boldsymbol{d} + \boldsymbol{n}, \tag{1}$$

with α_T a complex parameter accounting for channel propagation and backscattering effects from the target within the range-azimuth bin of interest, $\boldsymbol{p}(\nu_{d_T}) = [1, e^{j2\pi\nu_{d_T}}, \ldots, e^{j2\pi(N-1)\nu_{d_T}}]^T$, ν_{d_T} the normalized target Doppler frequency, $\boldsymbol{d}$ the N-dimensional column vector containing the filtered interfering echo samples, and $\boldsymbol{n}$ the N-dimensional column vector of the filtered noise samples.

The interfering vector $\boldsymbol{d}$ is the superposition of the returns from different uncorrelated point-like scatterers. It models clutter, non-threatening or threatening targets (different from the one of interest) contributions. Precisely, as depicted in Fig. 1, the vector $\boldsymbol{d}$ accounts for:

- clutter returns from different range-azimuth bins (r, l), with $r \in \{0, 1, \ldots, N_c\}$, $l \in \{0, 1, \ldots, L\}$, where $N_c \leq N - 1$ is the number of range rings that interfere with the range-azimuth bin of interest (0, 0), and $L + 1$ is the number of discrete azimuth sectors;
- echoes produced by non-threatening targets such as ground-moving vehicles, civil helicopters and aircrafts;
- echoes produced by threatening targets, previously acquired by the tracking processor, different from the one of interest.

As a consequence, the vector $\boldsymbol{d}$ can be expressed as:

$$\boldsymbol{d} = \sum_{k=1}^{N_t} \varrho_k \boldsymbol{J}^{r_k} \left(\boldsymbol{s} \odot \boldsymbol{p}(\nu_{d_k})\right), \tag{2}$$

where N_t is the total number of interfering scatterers, $r_k \in \{0, 1, \ldots, N-1\}$, ϱ_k, and ν_{d_k} are, respectively, the range position, the echo complex amplitude, and the normalized Doppler frequency of the k-th scatterer. Furthermore, $\forall r \in \{-N+1, \ldots, 0, \ldots, N-1\}$

$$J^r(l_1, l_2) = \begin{cases} 1 & \text{if } l_1 - l_2 = r \\ 0 & \text{if } l_1 - l_2 \neq r \end{cases} \quad (l_1, l_2) \in \{1, \ldots, N\}^2$$

denotes the shift matrix, and $\boldsymbol{J}^{-r} = \boldsymbol{J}^{rT}$.

According to (2), the output of the matched filter to the target signature $\boldsymbol{s} \odot \boldsymbol{p}(\nu_{d_T})$, is given by:

$$\begin{aligned}\left(\boldsymbol{s} \odot \boldsymbol{p}(\nu_{d_T})\right)^\dagger \boldsymbol{v} &= \alpha_T \|\boldsymbol{s}\|^2 + \left(\boldsymbol{s} \odot \boldsymbol{p}(\nu_{d_T})\right)^\dagger \boldsymbol{n} \\ &\quad + \sum_{k=1}^{N_t} \varrho_k \left(\boldsymbol{s} \odot \boldsymbol{p}(\nu_{d_T})\right)^\dagger \boldsymbol{J}^{r_k} \left(\boldsymbol{s} \odot \boldsymbol{p}(\nu_{d_k})\right). \end{aligned} \tag{3}$$

In the following, we assume that the vector $\boldsymbol{n}$, uncorrelated from $\boldsymbol{d}$, is a zero-mean, complex circular white noise, i.e.: $\mathbb{E}[\boldsymbol{n}] = 0$ and $\mathbb{E}[\boldsymbol{n}\boldsymbol{n}^\dagger] = \sigma_n^2 \boldsymbol{I}$. We denote by $\sigma_k^2 = \mathbb{E}[|\varrho_k|^2]$ the echo mean power, produced by the k-th scatterer. Furthermore, we model the normalized Doppler frequency ν_{d_k} as a random variable uniformly distributed around a mean Doppler frequency $\bar{\nu}_{d_k}$, i.e., $\nu_{d_k} \sim \mathcal{U}(\bar{\nu}_{d_k} - \frac{\epsilon_k}{2}, \bar{\nu}_{d_k} + \frac{\epsilon_k}{2})$. Consequently, since the scatterers and the noise are uncorrelated, the disturbance power at the output of the matched filter is given by

$$\begin{aligned}&\mathbb{E}\left[\left|\left(\boldsymbol{s} \odot \boldsymbol{p}(\nu_{d_T})\right)^\dagger \boldsymbol{n} \right.\right. \\ &\qquad \left.\left. + \sum_{k=1}^{N_t} \varrho_k \left(\boldsymbol{s} \odot \boldsymbol{p}(\nu_{d_T})\right)^\dagger \boldsymbol{J}^{r_k} \left(\boldsymbol{s} \odot \boldsymbol{p}(\nu_{d_k})\right)\right|^2\right] \\ &\quad = \mathbb{E}\left[\left|\left(\boldsymbol{s} \odot \boldsymbol{p}(\nu_{d_T})\right)^\dagger \boldsymbol{n}\right|^2\right] \\ &\qquad + \mathbb{E}\left[\left|\sum_{k=1}^{N_t} \varrho_k \left(\boldsymbol{s} \odot \boldsymbol{p}(\nu_{d_T})\right)^\dagger \boldsymbol{J}^{r_k} \left(\boldsymbol{s} \odot \boldsymbol{p}(\nu_{d_k})\right)\right|^2\right] \\ &\quad = \sum_{k=1}^{N_t} \sigma_k^2 \|\boldsymbol{s}\|^2 \mathbb{E}\left[\mathrm{g}_{\boldsymbol{s}}\left(r_k, \nu_{d_k} - \nu_{d_T}\right)\right] + \sigma_n^2 \|\boldsymbol{s}\|^2, \end{aligned} \tag{4}$$

where

$$\mathrm{g}_{\boldsymbol{s}}(r, \nu) = \frac{1}{\|\boldsymbol{s}\|^2} \left|\boldsymbol{s}^\dagger \boldsymbol{J}^r \left(\boldsymbol{s} \odot \boldsymbol{p}(\nu)\right)\right|^2 \tag{5}$$

is the slow-time ambiguity function of the code $\boldsymbol{s}$, with $r \in \{0, 1, \ldots, N-1\}$ the time-lag[1] and $\nu \in [-\frac{1}{2}, \frac{1}{2}]$ the normalized Doppler frequency. Precisely, for a given value of r, $\mathrm{g}_{\boldsymbol{s}}(r, \nu)$ gives the Doppler response to an interfering patch located $r \times$PRI away from the one of interest.

[1]Notice that, between the range position and the time-lag there exists a one-to-one mapping. Thus, in the following we will use interchangeably both the terms.

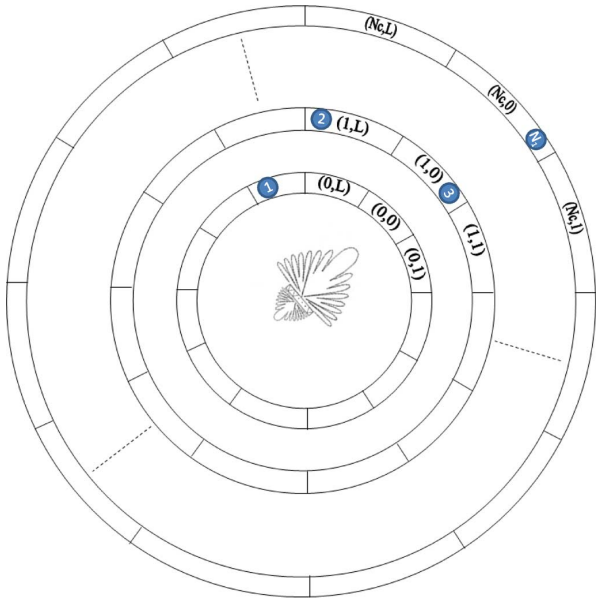

Fig. 1. Non-threatening and threatening targets, represented by blue circles, together with range-azimuth bins of the illuminated area around the radar antenna pattern.

A. Information for Cognitive Processing

Based on (4), to characterize the mean disturbance power at the output of the filter matched to the target signature, we need the mean power σ_k^2 as well as the Doppler parameters $\bar{\nu}_{d_k}$ and ϵ_k of each scatterer. This information can be obtained according to a cognitive paradigm. If the k-th point-like scatterer models the return from the clutter range-azimuth bin (r,l), as shown in [12], [20], its Radar Cross Section (RCS) $\sigma_0^{(r,l)}$ can be predicted through the interaction between a digital terrain map, such as the National Land Cover Data (NLCD), and RCS clutter models, see [21], [22], ([23], Ch. 15, 16). Whenever $\sigma_0^{(r,l)}$ has been estimated, we can evaluate the corresponding σ_k^2 as:

$$\sigma_k^2 = \sigma_0^{(r,l)} L_{r_k} \left|G(\theta_k)\right|^2, \tag{6}$$

where L_{r_k} is a constant accounting for the channel propagation effects, such as the free space two-way path loss and additional system losses (radar equation), θ_k is the azimuth angle of the bin (r,l), and $G(\theta)$ is the one-way antenna gain for the angle[2] θ. To define the mean clutter Doppler frequency $\bar{\nu}_{d_k}$ and the uncertainty ϵ_k on the clutter Doppler extension, associated with the (r,l)-th range-azimuth bin, a meaningful criterion is to fix $\bar{\nu}_{d_k}$ equal to the frequency peak of the clutter Power Spectral Density (PSD) (characterizing the (r,l)-th bin) and to take ϵ_k equal to the 90/95-percent power bandwidth. Again, we can make use of NLCD to classify each bin and, consequently, to determine an adequate model of the corresponding clutter PSD. For instance, it has been shown in [24], [25] that the exponential model is among the most accurate approximations for the windblown ground-clutter spectral measurements.

With reference to both threatening and non-threatening targets, we can obtain information about their parameters exploiting the track files managed by the radar system. For threatening targets, these files are required in order to predict target trajectories; these predictions are fundamental for defense applications in the fields of airborne early warning and homeland security. For non-threatening targets, as explained in [32], these files are required to avoid wasting radar timeline. In fact, for an appropriate allocation of the resources, the radar system firstly identifies and classifies the confirmed target, analyzing its amplitude and Doppler characteristics. If the target is defined to be threatening rather than benign, a track file in the search-and-track modality is opened; otherwise, a track-while-scan mode is used to maintain the track, avoiding the activation of a new qualification process to each scan and the consequent consume of large amounts of radar resources. Thus, accessing to these continuously updated track files (new measurements are made in each scan), for each threatening or non-threatening target, cognitive estimates of its RCS, position, and normalized Doppler frequency can be acquired.

B. Problem Formulation

In the following, without loss of generality, we center the Doppler frequency axis in the target Doppler frequency, namely all the normalized Doppler frequencies are expressed in terms of the difference with respect to ν_{d_T}. Furthermore, we discretize the normalized Doppler interval $[-\frac{1}{2},\frac{1}{2}[$, into N_ν bins, represented by the discrete frequencies $\nu_h = -\frac{1}{2} + \frac{h}{N_\nu}$, $h = 0,\dots N_\nu - 1$. Thus, each statistical expectation

$$\mathbb{E}\left[\mathrm{g}_{\boldsymbol{s}}\left(r_k,\nu_{d_k}\right)\right]$$

can be approximated with the sample mean over the Doppler bins intersecting $[\bar{\nu}_{d_k} - \frac{\epsilon_k}{2}, \bar{\nu}_{d_k} + \frac{\epsilon_k}{2}] = I_k$, namely

$$\mathbb{E}\left[\mathrm{g}_{\boldsymbol{s}}\left(r_k,\nu_{d_k}\right)\right] \approx \frac{1}{Card(B_k)} \sum_{h\in B_k} \mathrm{g}_{\boldsymbol{s}}(r_k,\nu_h) \tag{7}$$

where $B_k = \{h : [\nu_h - \frac{1}{2N_\nu}, \nu_h + \frac{1}{2N_\nu}[\cap I_k \neq \emptyset\}$, namely, it is the set containing the Doppler bin indices associated with the k-th scatterer[3]. Based on (7) and associating to each range-Doppler bin the corresponding interference power, the total disturbance power at the output of the matched filter (given in (4)) can be expressed as

$$\begin{aligned}
&\sum_{k=1}^{N_t} \sigma_k^2 \|\boldsymbol{s}\|^2 \left(\frac{1}{Card(B_k)} \sum_{h\in B_k} \mathrm{g}_{\boldsymbol{s}}(r_k,\nu_h)\right) + \sigma_n^2\|\boldsymbol{s}\|^2 \\
&\quad = \sum_{r=0}^{N-1}\sum_{k=1}^{N_t} \sigma_k^2\|\boldsymbol{s}\|^2 \\
&\qquad \times \left(\frac{1}{Card(B_k)} \sum_{h\in B_k} \delta(r-r_k)\mathrm{g}_{\boldsymbol{s}}(r,\nu_h)\right) + \sigma_n^2\|\boldsymbol{s}\|^2 \\
&\quad = \sum_{r=0}^{N-1}\sum_{h=0}^{N_\nu-1} \|\boldsymbol{s}\|^2 \mathrm{g}_{\boldsymbol{s}}(r,\nu_h) \\
&\qquad \times \left(\sum_{k=1}^{N_t} \delta(r-r_k)\mathbf{1}_{B_k}(h)\frac{\sigma_k^2}{Card(B_k)}\right) + \sigma_n^2\|\boldsymbol{s}\|^2 \\
&\quad = \sum_{r=0}^{N-1}\sum_{h=0}^{N_\nu-1} p_{(r,h)}\|\boldsymbol{s}\|^2 \mathrm{g}_{\boldsymbol{s}}(r,\nu_h) + \sigma_n^2\|\boldsymbol{s}\|^2,
\end{aligned} \tag{8}$$

[2]We are considering, for notational simplicity, a two-dimensional scenario (the generalization to the three-dimensional case is straightforward).

[3]Notice that, the set of Doppler frequencies $[-\frac{1}{2},-\frac{1}{2}+\frac{1}{2N_\nu}[\cup[\frac{1}{2}-\frac{1}{2N_\nu},\frac{1}{2}[$ corresponds to $h = 0$.

where, $\delta(\cdot)$ is the Kronecker delta function, $\mathbf{1}_A(x)$ denotes the indicator function of the set A, and

$$p_{(r,h)} = \sum_{k=1}^{N_t} \delta(r - r_k)\mathbf{1}_{B_k}(h)\frac{\sigma_k^2}{Card(B_k)},$$

is the range-Doppler interference map, namely, for each range-Doppler bin (r, ν_h), $p_{(r,h)}$ is interference power in that bin. Notice that, in the range-Doppler regions free of interference $p_{(r,h)} = 0$.

Based on the aforementioned model, in this paper we deal with the design of a suitable radar waveform minimizing the disturbance power at the output of the matched filter. This is tantamount[4] to shaping the ambiguity function of the transmitted signal so as to exhibit low values in range-Doppler bins where strong unwanted returns are foreseen. To be compliant with today amplifier technology, we also force a constant modulus constraint, obtaining phase-only modulated waveforms. Precisely, we consider both continuous and finite alphabet codes. As to the continuous alphabet case, we assume that:

$$\boldsymbol{s} \in \Omega_\infty, \tag{9}$$

where $\Omega_\infty = \{\boldsymbol{x} \in \mathbb{C}^N \,|\, |x(i)| = 1, i = 1, \ldots, N|\}$. Besides, with reference to the discrete alphabet case, we suppose

$$\boldsymbol{s} \in \Omega_M, \tag{10}$$

where $\Omega_M = \{\boldsymbol{s} : \boldsymbol{s}(i) \in \Psi_M\}$ with $\Psi_M = \{1, \varpi, \ldots, \varpi^{M-1} \,|\, \varpi = e^{j\frac{2\pi}{M}}\}$.

Summarizing, the design of a radar code sharing a desired ambiguity function, can be formulated as the following constrained optimization problems:

$$\mathrm{P}^\infty \begin{cases} \min\limits_{\boldsymbol{s}} & \phi(\boldsymbol{s}) \\ \text{s.t.} & \boldsymbol{s} \in \Omega_\infty \end{cases}, \quad \mathrm{P}^M \begin{cases} \min\limits_{\boldsymbol{s}} & \phi(\boldsymbol{s}) \\ \text{s.t.} & \boldsymbol{s} \in \Omega_M \end{cases}, \tag{11}$$

where

$$\phi(\boldsymbol{s}) = \sum_{r=0}^{N-1}\sum_{h=0}^{N_\nu-1} p_{(r,h)}\|\boldsymbol{s}\|^2 \mathrm{g}_{\boldsymbol{s}}(r, \nu_h) \tag{12}$$

is the interference power at the output of the matched filter. Notice that, assuming a uniform interference power among the interfering bins (homogeneous interference scenario), a robust phase code design can be performed, for which we only need to locate the range-Doppler bins where strong unwanted returns are foreseen. Furthermore, it is worth pointing out that the proposed design requires the specification of the target doppler ν_{d_T}; as a consequence, the radar code $\boldsymbol{s}^\star$ depends on this pre-assigned value. Some applicability scenarios are now described:

1 Assume that, after an uncoded (or a possibly standard coded) transmission a detection is declared in a given Doppler bin, using a high value of the false alarm Probability (P_{fa}). Then, our design approach can be employed to cognitively shape the waveform for the next transmission in order to confirm the detection in the previously identified bin, possibly with a smaller value of the P_{fa} (confirmation process), [32].

2 A radar code optimized to an average scenario, with respect to the target Doppler frequency, can be selected. In this case, denoting by $\psi^i(\boldsymbol{s}),\ i = 1, \ldots, N_d$ the output interference power corresponding to the target Doppler frequency $\nu^i_{d_T},\ i = 1, \ldots, N_d$, the continuous/discrete phase radar code might be chosen as a solution to the following problems:

$$\bar{\mathrm{P}}^\infty \begin{cases} \min\limits_{\boldsymbol{s}} & \frac{1}{N_d}\sum\limits_{i=1}^{N_d}\psi^i(\boldsymbol{s}) \\ \text{s.t.} & \boldsymbol{s} \in \Omega_\infty \end{cases}, \quad \bar{\mathrm{P}}^M \begin{cases} \min\limits_{\boldsymbol{s}} & \frac{1}{N_d}\sum\limits_{i=1}^{N_d}\psi^i(\boldsymbol{s}) \\ \text{s.t.} & \boldsymbol{s} \in \Omega_M. \end{cases} \tag{13}$$

Remark 1: Notice that the proposed framework can be also applied to fast-time coding. In this case, the problem of shaping the range-Doppler signal response becomes that of minimizing the volume of the classic ambiguity function in some regions of the range-Doppler plane (under the constant modulus waveform constraint). This problem has been of interest among the radar community [6] since the late sixties; however, the optimization theory was not yet very mature to provide the instruments to handle such hard problem. In this context, we would remark the approach followed in [5] where a heuristic algorithm based on a set of nonlinear variational equations (whose solution has been obtained using iterative Newton-Raphson techniques), is proposed.

Remark 2: For the considered reverberating environment, we could also deal with the joint design of the transmitted phase code $\boldsymbol{s} \in \mathbb{C}^N$ and receive filter $\boldsymbol{h} \in \mathbb{C}^N$ optimizing (over $\boldsymbol{s}$ and $\boldsymbol{h}$) the Signal to Interference plus Noise Ratio (SINR) at the filter output [2], [3]. Otherwise stated, we can formulate the following joint design optimization:

$$\mathrm{P}_{\{\boldsymbol{s},\boldsymbol{h}\}} \begin{cases} \max\limits_{\boldsymbol{s},\boldsymbol{h}} & \dfrac{\left|\boldsymbol{h}^\dagger\left(\boldsymbol{s}\odot\boldsymbol{p}(\nu_{d_T})\right)\right|^2}{\sum\limits_{k=1}^{N_t}\sigma_k^2\mathbb{E}\left[\left|\boldsymbol{h}^\dagger\boldsymbol{J}^{r_k}\left(\boldsymbol{s}\odot\boldsymbol{p}(\nu_{d_k})\right)\right|^2\right] + \sigma_n^2\|\boldsymbol{h}\|^2} \\ \text{s.t.} & \boldsymbol{s} \in \Omega_\infty \ \ (\text{resp. } \Omega_M) \end{cases}. \tag{14}$$

Problem $\mathrm{P}_{\{\boldsymbol{s},\boldsymbol{h}\}}$ is generally NP-hard and iterative algorithms, such as those in [33]–[35], and [36], can be used to get a feasible (high quality) transmitted signal and receive filter pair. A simplified and, usually, more practical design method relies on the exploitation, at the transmitter end, of a general purpose probing waveform (with desired radar behavior) and the application at the receiver end of some specific filters (also referred to as mismatched filters [37] or instrumental variable filters [38]), optimizing radar performance metrics like the Integrated Sidelobe Level (ISL), Peak to Sidelobe Level (PSL), SINR [39], or their combination. However, the coefficients of the resulting filters could share an unacceptable dynamic range and this drawback could reduce their practical effectiveness.

Another simplified design approach is based on using a matched filter at the receiver end, namely the receive filter maximizing the peak Signal to Noise Ratio (SNR) (i.e., $\boldsymbol{h} = \boldsymbol{s}$), and synthesizing the transmitted signal which optimizes the SINR in (14). In this context, the maximization of the SINR is tantamount to shaping the transmitted waveform ambiguity function, namely the design criterion considered in (11).

Based on above considerations, it is clear that, accounting for a joint signal and filter design, we can obtain in general higher SINR values than those ensured by the previously specified suboptimum techniques (especially in highly non-symmetric clutter environments). Nevertheless, exploiting the approach (11), we

[4]Whenever the transmitted energy $\|\boldsymbol{s}\|^2$ has been fixed, the noise contribution to the overall disturbance power is independent of the transmitted waveform.

are able to synthesize a phase-only filter, hence to directly overcome the dynamic range issues concerning filter implementation. Additionally, considering at the design stage the set Ω_2, namely forcing the transmitted code and receive filter to be binary sequences, we can also reduce the computational complexity connected with filtering operation; in fact for binary transmit/receive pairs the convolution just requires summations.

We also point out that, employing the proposed design approach (11), the range-Doppler bins, where strong unwanted returns are foreseen, experience a double suppression effect (both at transmission and at reception), as compared with the receiver only design technique. Besides, we can further improve the SINR performance of the waveform designed according to (11) applying a mismatched filter at the receiver end (possibly we could also iterate the flip-flop procedure). As a matter of fact, a waveform devised according to (11) can represent a good initial point for iterative algorithms involved in the solution of (14). Finally, since "similarity" codes [40] sharing suitable ambiguity functions are often required in fully cognitive architectures, [20], [33], the design criterion (11) can be reasonably exploited to synthesize appropriate reference codes.

III. Design Issues

In this section we focus on the study of P^{∞} and P^{M}, which define non-convex optimization problems as the constraint sets Ω_{∞} and Ω_M are non-convex sets. Furthermore, the objective function $\phi(\boldsymbol{s})$ is generally a non-convex function. In fact, considering for instance $N = 3$, N_ν even, and

$$p_{(r,h)} = \begin{cases} 1 & (r,h) = \left(1, \frac{N_\nu}{2}\right) \\ 0 & \text{otherwise} \end{cases},$$

it is not difficult to show that

$$\begin{aligned}\phi_1(\boldsymbol{s}) &= \sum_{r=0}^{N-1}\sum_{h=0}^{N_\nu-1} p_{(r,h)}\|\boldsymbol{s}\|^2 \mathrm{g}_{\boldsymbol{s}}(r,\nu_h) = |\boldsymbol{s}^\dagger \boldsymbol{J}^1 \boldsymbol{s}|^2 \\ &= |\boldsymbol{s}(1)\bar{\boldsymbol{s}}(2) + \boldsymbol{s}(2)\bar{\boldsymbol{s}}(3)|^2,\end{aligned}$$

is a non-convex function. To this end, let us consider the points $\boldsymbol{s}^1 = [a, 0, a]^T$ and $\boldsymbol{s}^2 = [-a, -1, a]^T$, with $a > 0$. Obviously, $\phi_1(\boldsymbol{s}^1) = \phi_1(\boldsymbol{s}^2) = 0$; moreover, since $\phi_1(\boldsymbol{s}) \geq 0\ \forall \boldsymbol{s} \in \mathbb{C}^N$, if $\phi_1(\boldsymbol{s})$ were convex, then $\phi_1(\lambda \boldsymbol{s}^1 + (1-\lambda)\boldsymbol{s}^2) = 0,\ \forall \lambda \in [0,1]$. This is not true because $\phi_1(\lambda \boldsymbol{s}^1 + (1-\lambda)\boldsymbol{s}^2) = 4|1-\lambda|^2|a|^2|\lambda^2| \neq 0,\ \forall \lambda \in]0,1[$, and thus $\phi_1(\boldsymbol{s})$ is a non-convex function.

As explained in Appendix A-1, a real valued conjugate homogeneous quartic function associated with the complex vector variable $\boldsymbol{s} \in \mathbb{C}^N$, is defined as

$$f(\boldsymbol{s}) = \sum_{r_1=1}^{R_1} |\boldsymbol{s}^\dagger \boldsymbol{A}^{r_1} \boldsymbol{s}|^2 - \sum_{r_1=R_1+1}^{R_2} |\boldsymbol{s}^\dagger \boldsymbol{A}^{r_1} \boldsymbol{s}|^2 \qquad (15)$$

where $\boldsymbol{A}^{r_1} \in \mathbb{C}^{N,N}$ and $r_1 = 1, \ldots, R_1, \ldots, R_2$. This implies that the objective function of problems P^{∞} and P^{M}

$$\phi(\boldsymbol{s}) = \sum_{r=0}^{N-1}\sum_{h=0}^{N_\nu-1} p_{(r,h)} \left|\boldsymbol{s}^\dagger \boldsymbol{J}^r \mathbf{diag}\left(\boldsymbol{p}(\nu_h)\right)\boldsymbol{s}\right|^2,$$

belongs to the aforementioned class. In fact, $\phi(\boldsymbol{s})$ can be expressed as in (15) taking $R_2 = 0$, $R_1 = NN_\nu$, considering a one-to-one mapping[5], $\Upsilon : r_1 \in \{1, \ldots, R_1\} \rightarrow (r,h) \in \{0, N-1\} \times \{0, N_\nu - 1\}$, and taking $\boldsymbol{A}^{r_1} = \sqrt{p_{(r,h)}}\boldsymbol{J}^r \mathbf{diag}\left(\boldsymbol{p}(\nu_h)\right)$. Consequently, problems P^{∞} and P^{M} belong to the class of complex quartic minimization problems

$$\mathrm{CQ}^{\infty} \begin{cases} \min\limits_{\boldsymbol{s}} & f(\boldsymbol{s}) \\ \text{s.t.} & \boldsymbol{s} \in \Omega_{\infty} \end{cases}, \quad \mathrm{CQ}^{M} \begin{cases} \min\limits_{\boldsymbol{s}} & f(\boldsymbol{s}) \\ \text{s.t.} & \boldsymbol{s} \in \Omega_{M}. \end{cases} \qquad (16)$$

The following theorem illustrates the hardness of the problems CQ^{∞} and CQ^{M}:

Theorem 3.1: Problems CQ^{∞} and CQ^{M} are NP-hard in general.

Proof: See Appendix B. ∎

Based on the previous theorem, in the following subsection, we focus on the design of suitable techniques capable of providing, in polynomial time, some good quality solutions to problems CQ^{∞} and CQ^{M}, and thus to P^{∞} and P^{M}.

A. Maximum Block Improvement Method

In this subsection, we devise three MBI type optimization algorithms, which try to locally improve the objective function in CQ^{∞} and in CQ^{M}. As already highlighted, the MBI method is an iterative algorithm known to achieve excellent performance in the maximization of real polynomial functions subject to spherical constraints [19]. Moreover, it was proved that the sequence produced by the MBI method converges to a stationary point for the relaxed multi-linear problem [19]; however, such stationary point is not ensured being a globally optimal solution.

Before proceeding further with the design of our MBI type algorithms, we point out that, for any finite value λ, problems CQ^{∞} and CQ^{M} share the same (local) optimal solutions, respectively, of

$$\widetilde{\mathrm{CQ}}_{\lambda}^{\infty} \begin{cases} \max\limits_{\boldsymbol{s}} & \lambda(\boldsymbol{s}^\dagger \boldsymbol{s})^2 - f(\boldsymbol{s}) \\ \text{s.t.} & \boldsymbol{s} \in \Omega_{\infty} \end{cases}, \quad \widetilde{\mathrm{CQ}}_{\lambda}^{M} \begin{cases} \max\limits_{\boldsymbol{s}} & \lambda(\boldsymbol{s}^\dagger \boldsymbol{s})^2 - f(\boldsymbol{s}) \\ \text{s.t.} & \boldsymbol{s} \in \Omega_{M}. \end{cases} \qquad (17)$$

In fact, since $(\boldsymbol{s}^\dagger \boldsymbol{s})^2 = N^2$ is a constant function whenever $\boldsymbol{s} \in \Omega_{\infty}$ (resp. $\boldsymbol{s} \in \Omega_M$), CQ^{∞} (resp. CQ^{M}) is equivalent to $\widetilde{\mathrm{CQ}}_{\lambda}^{\infty}$ (resp. $\widetilde{\mathrm{CQ}}_{\lambda}^{M}$). Thus in the following, we focus on problems $\widetilde{\mathrm{CQ}}_{\lambda}^{\infty}$ and $\widetilde{\mathrm{CQ}}_{\lambda}^{M}$.

The first algorithm we propose, exploits the conjugate-super-symmetric tensor representation of the complex quartic functions, see Appendix A-3. Precisely, suppose that $f(\boldsymbol{s})$ is a complex quartic function in the form (15) and let $\mathcal{G}^{\lambda}$ be the conjugate-super-symmetric tensor form such that

$$\mathcal{G}^{\lambda}\left(\begin{pmatrix}\boldsymbol{s}\\ \bar{\boldsymbol{s}}\end{pmatrix}, \begin{pmatrix}\boldsymbol{s}\\ \bar{\boldsymbol{s}}\end{pmatrix}, \begin{pmatrix}\boldsymbol{s}\\ \bar{\boldsymbol{s}}\end{pmatrix}, \begin{pmatrix}\boldsymbol{s}\\ \bar{\boldsymbol{s}}\end{pmatrix}\right) = \lambda(\boldsymbol{s}^\dagger \boldsymbol{s})^2 - f(\boldsymbol{s}). \qquad (18)$$

Hence, we introduce an MBI type method with a linear-improvement subroutine[6] for $\widetilde{\mathrm{CQ}}_{\lambda}^{\infty}$ (resp. $\widetilde{\mathrm{CQ}}_{\lambda}^{M}$), as described in **Algorithm MBIL**.

[5]The existence of such a correspondence is ensured by the equinumerosity of two sets $\{1, \ldots, NN_\nu\}$ and $\{0, N-1\} \times \{0, N_\nu - 1\}$.

[6]Notice that, $\mathcal{G}^{\lambda}(\boldsymbol{y}, \binom{\boldsymbol{s}_k^2}{\bar{\boldsymbol{s}}_k^2}, \binom{\boldsymbol{s}_k^3}{\bar{\boldsymbol{s}}_k^3}, \binom{\boldsymbol{s}_k^4}{\bar{\boldsymbol{s}}_k^4}) = \boldsymbol{c}^{1T}\boldsymbol{y}$ is a linear function in the variable $\boldsymbol{y}$, and we denote by $\boldsymbol{c}^1 \rightarrow \mathcal{G}^{\lambda}(\cdot, \binom{\boldsymbol{s}_k^2}{\bar{\boldsymbol{s}}_k^2}, \binom{\boldsymbol{s}_k^3}{\bar{\boldsymbol{s}}_k^3}, \binom{\boldsymbol{s}_k^4}{\bar{\boldsymbol{s}}_k^4})$ the vector associated with the linear function on the right side of the arrow. Similarly, we proceed for the other variables.

Algorithm MBIL: MBI method with a linear-improvement subroutine for $\widetilde{\mathrm{CQ}}_{\lambda}^{\infty}$ (resp. $\widetilde{\mathrm{CQ}}_{\lambda}^{M}$)

0 (Initialization): Generate, possibly randomly, $(\boldsymbol{s}_0^1, \boldsymbol{s}_0^2, \boldsymbol{s}_0^3, \boldsymbol{s}_0^4)$ with $\boldsymbol{s}_0^m \in \Omega_\infty$ (resp. Ω_M) for $m = 1, 2, 3, 4$, and compute the initial objective value $v_0 = \mathcal{G}^\lambda((\begin{smallmatrix}\boldsymbol{s}_0^1\\ \bar{\boldsymbol{s}}_0^1\end{smallmatrix}), (\begin{smallmatrix}\boldsymbol{s}_0^2\\ \bar{\boldsymbol{s}}_0^2\end{smallmatrix}), (\begin{smallmatrix}\boldsymbol{s}_0^3\\ \bar{\boldsymbol{s}}_0^3\end{smallmatrix}), (\begin{smallmatrix}\boldsymbol{s}_0^4\\ \bar{\boldsymbol{s}}_0^4\end{smallmatrix}))$. Set $k = 0$.

1 (Block Linear Improvement): Let

$\boldsymbol{c}^1 \rightarrow \mathcal{G}^\lambda(\cdot, (\begin{smallmatrix}\boldsymbol{s}_k^2\\ \bar{\boldsymbol{s}}_k^2\end{smallmatrix}), (\begin{smallmatrix}\boldsymbol{s}_k^3\\ \bar{\boldsymbol{s}}_k^3\end{smallmatrix}), (\begin{smallmatrix}\boldsymbol{s}_k^4\\ \bar{\boldsymbol{s}}_k^4\end{smallmatrix}))$, $\boldsymbol{c}^2 \rightarrow$
$\mathcal{G}^\lambda((\begin{smallmatrix}\boldsymbol{s}_k^1\\ \bar{\boldsymbol{s}}_k^1\end{smallmatrix}), \cdot, (\begin{smallmatrix}\boldsymbol{s}_k^3\\ \bar{\boldsymbol{s}}_k^3\end{smallmatrix}), (\begin{smallmatrix}\boldsymbol{s}_k^4\\ \bar{\boldsymbol{s}}_k^4\end{smallmatrix}))$,
$\boldsymbol{c}^3 \rightarrow \mathcal{G}^\lambda((\begin{smallmatrix}\boldsymbol{s}_k^1\\ \bar{\boldsymbol{s}}_k^1\end{smallmatrix}), (\begin{smallmatrix}\boldsymbol{s}_k^2\\ \bar{\boldsymbol{s}}_k^2\end{smallmatrix}), \cdot, (\begin{smallmatrix}\boldsymbol{s}_k^4\\ \bar{\boldsymbol{s}}_k^4\end{smallmatrix}))$, $\boldsymbol{c}^4 \rightarrow$
$\mathcal{G}^\lambda((\begin{smallmatrix}\boldsymbol{s}_k^1\\ \bar{\boldsymbol{s}}_k^1\end{smallmatrix}), (\begin{smallmatrix}\boldsymbol{s}_k^2\\ \bar{\boldsymbol{s}}_k^2\end{smallmatrix}), (\begin{smallmatrix}\boldsymbol{s}_k^3\\ \bar{\boldsymbol{s}}_k^3\end{smallmatrix}), \cdot)$,

be the vectors associated with the linear functions on the right side of the arrows.

For $m = 1, 2, 3, 4$ let

$\boldsymbol{y}_{k+1}^m = \arg\max_{\boldsymbol{s}\in\Omega_\infty} (\begin{smallmatrix}\boldsymbol{s}\\ \bar{\boldsymbol{s}}\end{smallmatrix})^T \boldsymbol{c}^m$ (resp. $\boldsymbol{y}_{k+1}^m = \arg\max_{\boldsymbol{s}\in\Omega_M} (\begin{smallmatrix}\boldsymbol{s}\\ \bar{\boldsymbol{s}}\end{smallmatrix})^T \boldsymbol{c}^m$), $w_{k+1}^m = (\begin{smallmatrix}\boldsymbol{y}_{k+1}^m\\ \bar{\boldsymbol{y}}_{k+1}^m\end{smallmatrix})^T \boldsymbol{c}^m$.

2 (Maximum Improvement): Let $w_{k+1} = \max_{1\le m\le 4} w_{k+1}^m$ and $m^* = \arg\max_{1\le m\le 4} w_{k+1}^m$. Replace $\boldsymbol{s}_{k+1}^m = \boldsymbol{s}_k^m$ for all $m \neq m^*$, $\boldsymbol{s}_{k+1}^{m^*} = \boldsymbol{y}_{k+1}^{m^*}$ and $v_{k+1} = w_{k+1}$.

3 (Stopping Criterion): If $|\frac{v_{k+1}-v_k}{\max(1,v_k)}| < \epsilon$, stop. Otherwise, set $k = k + 1$, and go to step 1.

4 (Output): For $1 \le n \le 4$, let

$t^n = \mathcal{G}^\lambda((\begin{smallmatrix}\boldsymbol{s}_{k+1}^n\\ \bar{\boldsymbol{s}}_{k+1}^n\end{smallmatrix}), (\begin{smallmatrix}\boldsymbol{s}_{k+1}^n\\ \bar{\boldsymbol{s}}_{k+1}^n\end{smallmatrix}), (\begin{smallmatrix}\boldsymbol{s}_{k+1}^n\\ \bar{\boldsymbol{s}}_{k+1}^n\end{smallmatrix}), (\begin{smallmatrix}\boldsymbol{s}_{k+1}^n\\ \bar{\boldsymbol{s}}_{k+1}^n\end{smallmatrix}))$,

$n^* = \arg\max_{1\le n\le 4} t^n$. Return t^{n^*} and $\boldsymbol{s}_{k+1}^{n^*}$.

Notice that the objective value at each iteration of the MBIL method is generally increasing except for the last step. This is because the returned t^{n^*} is the value of a polynomial function instead of the multi-linear form on which the MBIL algorithm is applied. We explicitly point out that, the issue of symmetry becomes quite delicate when dealing with complex polynomial functions and requires to introduce the concept of 'conjugate symmetry' (see Appendix A(-2 and -3)). Once the definitions of conjugate symmetry are given, we are in a position to extend the result obtained in ([26], Ch. 5) to the complex case:

Theorem 3.2: Suppose $g(\boldsymbol{s})$ is a convex complex quartic function and let $\mathcal{G}$ be the conjugate-super-symmetric tensor form associated with $g(\boldsymbol{s})$; then

$$\mathcal{G}\left(\begin{pmatrix}\boldsymbol{s}^1\\ \bar{\boldsymbol{s}}^1\end{pmatrix}, \begin{pmatrix}\boldsymbol{s}^2\\ \bar{\boldsymbol{s}}^2\end{pmatrix}, \begin{pmatrix}\boldsymbol{s}^3\\ \bar{\boldsymbol{s}}^3\end{pmatrix}, \begin{pmatrix}\boldsymbol{s}^4\\ \bar{\boldsymbol{s}}^4\end{pmatrix}\right) \le \max\left\{\mathcal{G}\left(\begin{pmatrix}\boldsymbol{s}^1\\ \bar{\boldsymbol{s}}^1\end{pmatrix}, \begin{pmatrix}\boldsymbol{s}^1\\ \bar{\boldsymbol{s}}^1\end{pmatrix}, \begin{pmatrix}\boldsymbol{s}^1\\ \bar{\boldsymbol{s}}^1\end{pmatrix}, \begin{pmatrix}\boldsymbol{s}^1\\ \bar{\boldsymbol{s}}^1\end{pmatrix}\right), \mathcal{G}\left(\begin{pmatrix}\boldsymbol{s}^2\\ \bar{\boldsymbol{s}}^2\end{pmatrix}, \begin{pmatrix}\boldsymbol{s}^2\\ \bar{\boldsymbol{s}}^2\end{pmatrix}, \begin{pmatrix}\boldsymbol{s}^2\\ \bar{\boldsymbol{s}}^2\end{pmatrix}, \begin{pmatrix}\boldsymbol{s}^2\\ \bar{\boldsymbol{s}}^2\end{pmatrix}\right), \mathcal{G}\left(\begin{pmatrix}\boldsymbol{s}^3\\ \bar{\boldsymbol{s}}^3\end{pmatrix}, \begin{pmatrix}\boldsymbol{s}^3\\ \bar{\boldsymbol{s}}^3\end{pmatrix}, \begin{pmatrix}\boldsymbol{s}^3\\ \bar{\boldsymbol{s}}^3\end{pmatrix}, \begin{pmatrix}\boldsymbol{s}^3\\ \bar{\boldsymbol{s}}^3\end{pmatrix}\right), \mathcal{G}\left(\begin{pmatrix}\boldsymbol{s}^4\\ \bar{\boldsymbol{s}}^4\end{pmatrix}, \begin{pmatrix}\boldsymbol{s}^4\\ \bar{\boldsymbol{s}}^4\end{pmatrix}, \begin{pmatrix}\boldsymbol{s}^4\\ \bar{\boldsymbol{s}}^4\end{pmatrix}, \begin{pmatrix}\boldsymbol{s}^4\\ \bar{\boldsymbol{s}}^4\end{pmatrix}\right)\right\}.$$

Proof: See Appendix C. ∎

From the above theorem, the monotonicity of the MBIL algorithm lies in whether or not we can find λ such that $\lambda(\boldsymbol{s}^\dagger\boldsymbol{s})^2 - f(\boldsymbol{s})$ is convex. In this respect, it is important to study the convexity of a complex quartic function.

Theorem 3.3: Suppose $f(\boldsymbol{s})$ is a complex quartic function.

- If $f(\boldsymbol{s}) = \sum_{r_1=1}^{R_1} |\boldsymbol{s}^\dagger \boldsymbol{A}^{r_1} \boldsymbol{s}|^2 - \sum_{r_1=R_1+1}^{R_2} |\boldsymbol{s}^\dagger \boldsymbol{A}^{r_1} \boldsymbol{s}|^2$, then f is convex with respect to $\boldsymbol{s}$ if and only if
$$h(\boldsymbol{y}, \boldsymbol{z}) = \sum_{r_1=1}^{R_1} h_{r_1}(\boldsymbol{y}, \boldsymbol{z}) - \sum_{r_1=R_1+1}^{R_2} h_{r_1}(\boldsymbol{y}, \boldsymbol{z}) \ge 0, \quad \forall \boldsymbol{y}, \boldsymbol{z} \in \mathbb{C}^n \quad (19)$$
where
$$\begin{aligned} h_{r_1}(\boldsymbol{y}, \boldsymbol{z}) = {} & \boldsymbol{y}^\dagger \boldsymbol{A}^{r_1} \boldsymbol{y} \boldsymbol{z}^\dagger \boldsymbol{A}^{r_1\dagger} \boldsymbol{z} + \boldsymbol{y}^\dagger \boldsymbol{A}^{r_1} \boldsymbol{z} \boldsymbol{y}^\dagger \boldsymbol{A}^{r_1\dagger} \boldsymbol{z} \\ & + \boldsymbol{y}^\dagger \boldsymbol{A}^{r_1} \boldsymbol{z} \boldsymbol{z}^\dagger \boldsymbol{A}^{r_1\dagger} \boldsymbol{y} + \boldsymbol{z}^\dagger \boldsymbol{A}^{r_1} \boldsymbol{y} \boldsymbol{y}^\dagger \boldsymbol{A}^{r_1\dagger} \boldsymbol{z} \\ & + \boldsymbol{z}^\dagger \boldsymbol{A}^{r_1} \boldsymbol{y} \boldsymbol{z}^\dagger \boldsymbol{A}^{r_1\dagger} \boldsymbol{y} + \boldsymbol{z}^\dagger \boldsymbol{A}^{r_1} \boldsymbol{z} \boldsymbol{y}^\dagger \boldsymbol{A}^{r_1\dagger} \boldsymbol{y}, \\ & \forall \boldsymbol{y}, \boldsymbol{z} \in \mathbb{C}^N. \end{aligned}$$
- If $\mathcal{H}$ is the conjugate-partial-symmetric fourth order tensor form[7] such that $\mathcal{H}(\bar{\boldsymbol{s}}, \boldsymbol{s}, \bar{\boldsymbol{s}}, \boldsymbol{s}) = f(\boldsymbol{s})$, then f is convex with respect to $\boldsymbol{s}$ if and only if
$$4\mathcal{H}(\bar{\boldsymbol{y}}, \boldsymbol{y}, \bar{\boldsymbol{z}}, \boldsymbol{z}) + \mathcal{H}(\bar{\boldsymbol{y}}, \boldsymbol{z}, \bar{\boldsymbol{y}}, \boldsymbol{z}) + \mathcal{H}(\bar{\boldsymbol{z}}, \boldsymbol{y}, \bar{\boldsymbol{z}}, \boldsymbol{y}) \ge 0, \quad \forall \boldsymbol{y}, \boldsymbol{z} \in \mathbb{C}^N. \quad (20)$$
- If $\mathcal{G}$ is the conjugate-super-symmetric fourth order tensor form[8] such that $\mathcal{G}((\begin{smallmatrix}\boldsymbol{s}\\ \bar{\boldsymbol{s}}\end{smallmatrix}), (\begin{smallmatrix}\boldsymbol{s}\\ \bar{\boldsymbol{s}}\end{smallmatrix}), (\begin{smallmatrix}\boldsymbol{s}\\ \bar{\boldsymbol{s}}\end{smallmatrix}), (\begin{smallmatrix}\boldsymbol{s}\\ \bar{\boldsymbol{s}}\end{smallmatrix})) = f(\boldsymbol{s})$, then f is convex with respect to $\boldsymbol{s}$ if and only if
$$\mathcal{G}\left(\begin{pmatrix}\boldsymbol{y}\\ \bar{\boldsymbol{y}}\end{pmatrix}, \begin{pmatrix}\boldsymbol{y}\\ \bar{\boldsymbol{y}}\end{pmatrix}, \begin{pmatrix}\boldsymbol{z}\\ \bar{\boldsymbol{z}}\end{pmatrix}, \begin{pmatrix}\boldsymbol{z}\\ \bar{\boldsymbol{z}}\end{pmatrix}\right) \ge 0, \quad \forall \boldsymbol{y}, \boldsymbol{z} \in \mathbb{C}^N. \quad (21)$$

Proof: See Appendix D. ∎

Theorem 3.3 indicates that the convexity of a quartic function is equivalent to the non-negativity of a certain biquadratic function. We further notice that the biquadratic function corresponding to the quartic function $(\boldsymbol{s}^\dagger\boldsymbol{s})^2$ is $2\boldsymbol{y}^\dagger\boldsymbol{y}\boldsymbol{z}^\dagger\boldsymbol{z} + (\boldsymbol{y}^\dagger\boldsymbol{z} + \boldsymbol{z}^\dagger\boldsymbol{y})^2$, which is strictly positive whenever $\boldsymbol{y} \neq 0$ and $\boldsymbol{z} \neq 0$. Consequently, we can make any quartic function convex by adding $(\boldsymbol{s}^\dagger\boldsymbol{s})^2$ multiplied by a large enough constant λ.

Corollary 3.4: Suppose $f(\boldsymbol{s})$ is a quartic function represented in the form (15) and denote by $h(\boldsymbol{y}, \boldsymbol{z})$ the function defined in (19). Then $\lambda(\boldsymbol{s}^\dagger\boldsymbol{s})^2 - f(\boldsymbol{s})$ is convex in $\boldsymbol{s}$ if and only if the scalar λ complies with:

$$\lambda\left(2\boldsymbol{y}^\dagger\boldsymbol{y}\boldsymbol{z}^\dagger\boldsymbol{z} + (\boldsymbol{y}^\dagger\boldsymbol{z} + \boldsymbol{z}^\dagger\boldsymbol{y})^2\right) - h(\boldsymbol{y}, \boldsymbol{z}) \ge 0, \quad \forall\, \boldsymbol{y}, \boldsymbol{z} \in \mathbb{C}^N, \quad (22)$$

Furthermore, letting

$$\lambda^* = \max_{\|\boldsymbol{z}\|=1, \|\boldsymbol{y}\|=1} h(\boldsymbol{y}, \boldsymbol{z}), \quad (23)$$

for any $\lambda \ge \lambda^*/2$, $\lambda(\boldsymbol{s}^\dagger\boldsymbol{s})^2 - f(\boldsymbol{s})$ is convex in $\boldsymbol{s}$.

Proof: See Appendix E. ∎

[7]See Appendix A-2 for more details on conjugate-partial-symmetric fourth order tensor forms.

[8]See Appendix A-3 for more details on conjugate-super-symmetric fourth order tensor forms.

Thus, exploiting Corollary 3.4 and Theorem 3.2, we have that, for any complex quartic function $f(\boldsymbol{s})$, we can find a λ such that the devised MBIL algorithm is monotonically increasing. Otherwise stated, $\lambda = \lambda^*/2$, with λ^* given in (23), ensures the equivalence between problems (17) and their relaxed multilinear problems. Notice that, in order to compute λ^*, i.e. the maximum value of the biquadratic function $h(\boldsymbol{y}, \boldsymbol{z})$, the MBI algorithm proposed in [19] can be exploited. Finally, we explicitly point out that the quality of the solution can be improved repeatedly using **Algorithm MBIL**, setting each time $\boldsymbol{s}_0^1 = \boldsymbol{s}_0^2 = \boldsymbol{s}_0^3 = \boldsymbol{s}_0^4 = \boldsymbol{s}_{k+1}^{n^*}$ as new starting points, if further progress is still possible.

The second method we propose, exploits the conjugate-partial-symmetric tensor representation of the complex quartic functions, see Appendix A-2. To this end, let $f(\boldsymbol{s})$ be a complex quartic function in the form (15) and $\mathcal{H}^\lambda$ be the conjugate-partial-symmetric tensor form such that

$$\lambda(\boldsymbol{s}^\dagger \boldsymbol{s})^2 - f(\boldsymbol{s}) = \mathcal{H}^\lambda(\bar{\boldsymbol{s}}, \boldsymbol{s}, \bar{\boldsymbol{s}}, \boldsymbol{s}). \tag{24}$$

Hence, we introduce an MBI type method with a quadratic-improvement subroutine[9] for problem $\widetilde{\mathrm{CQ}}_\lambda^\infty$ (resp. $\widetilde{\mathrm{CQ}}_\lambda^M$), as described in **Algorithm MBIQ**.

Algorithm MBIQ: MBI method with a quadratic-improvement subroutine for $\widetilde{\mathrm{CQ}}_\lambda^\infty$ (resp. $\widetilde{\mathrm{CQ}}_\lambda^M$)

0 (Initialization): Generate, possibly randomly, $(\boldsymbol{s}_0^1, \boldsymbol{s}_0^2)$ with $s_0^m \in \Omega_\infty$ (resp. Ω_M) for $m = 1, 2$ and compute the initial objective value $v_0 = \mathcal{H}^\lambda(\bar{\boldsymbol{s}}_0^1, \boldsymbol{s}_0^1, \bar{\boldsymbol{s}}_0^2, \boldsymbol{s}_0^2)$. Set $k = 0$.

1 (Block Quadratic Improvement): Let

$$\boldsymbol{B}^1 \rightarrow \mathcal{H}^\lambda(\cdot, \cdot, \bar{\boldsymbol{s}}_k^2, \boldsymbol{s}_k^2),\ \boldsymbol{B}^2 \rightarrow \mathcal{H}^\lambda(\bar{\boldsymbol{s}}_k^1, \boldsymbol{s}_k^1, \cdot, \cdot),$$

be the matrices associated with the bilinear functions on the right side of the arrows.

For $m = 1, 2$ let

$\boldsymbol{y}_{k+1}^m = \arg\max_{\boldsymbol{s} \in \Omega_\infty} (\boldsymbol{s})^\dagger \boldsymbol{B}^m \boldsymbol{s}$ (resp. $\boldsymbol{y}_{k+1}^m = \arg\max_{\boldsymbol{s} \in \Omega_M} (\boldsymbol{s})^\dagger \boldsymbol{B}^m \boldsymbol{s}$), $w_{k+1}^m = (\boldsymbol{y}_{k+1}^m)^\dagger \boldsymbol{B}^m \boldsymbol{y}_{k+1}^m$.

2 (Maximum Improvement): Let $w_{k+1} = \max_{1 \le m \le 2} w_{k+1}^m$ and $m^* = \arg\max_{1 \le m \le 2} w_{k+1}^m$. Replace $\boldsymbol{s}_{k+1}^m = \boldsymbol{s}_k^m$ for all $m \neq m^*$, $\boldsymbol{s}_{k+1}^{m^*} = \boldsymbol{y}_{k+1}^{m^*}$ and $v_{k+1} = w_{k+1}$.

3 (Stopping Criterion): If $|\frac{v_{k+1} - v_k}{\max(1, v_k)}| < \epsilon$, stop. Otherwise, set $k = k + 1$, and go to step 1.

4 (Output): For $n = 1, 2$, let $t^n = \mathcal{H}^\lambda(\bar{\boldsymbol{s}}_{k+1}^n, \boldsymbol{s}_{k+1}^n, \bar{\boldsymbol{s}}_{k+1}^n, \boldsymbol{s}_{k+1}^n)$, $n^* = \arg\max_{n=1,2} t^n$.

Return t^{n^*} and $\boldsymbol{s}_{k+1}^{n^*}$.

Now we give a sufficient condition for monotonicity of the MBIQ method.

[9]Notice that, $\mathcal{H}^\lambda(\boldsymbol{y}_1, \boldsymbol{y}_2, \bar{\boldsymbol{s}}_k^2, \boldsymbol{s}_k^2) = \boldsymbol{y}_1^T \boldsymbol{B}^1 \boldsymbol{y}_2$ is a bilinear function in the variables $\boldsymbol{y}_1$ and $\boldsymbol{y}_2$, and we denote by $\boldsymbol{B}^1 \rightarrow \mathcal{H}^\lambda(\cdot, \cdot, \bar{\boldsymbol{s}}_k^2, \boldsymbol{s}_k^2)$ the matrix associated with the bilinear function on the right side of the arrow. Similarly we proceed for the other pair of variables.

Theorem 3.5: Consider the complex quartic function $f(\boldsymbol{s})$ and let $\mathcal{H}$ be the associated conjugate-partial-symmetric fourth order tensor form. Then,

$$2\mathcal{H}(\bar{\boldsymbol{y}}, \boldsymbol{y}, \bar{\boldsymbol{z}}, \boldsymbol{z}) + \mathcal{H}(\bar{\boldsymbol{y}}, \boldsymbol{z}, \bar{\boldsymbol{y}}, \boldsymbol{z}) + \mathcal{H}(\bar{\boldsymbol{z}}, \boldsymbol{y}, \bar{\boldsymbol{z}}, \boldsymbol{y}) \ge 0, \quad \forall \boldsymbol{y}, \boldsymbol{z} \in \mathbb{C}^N \tag{25}$$

implies

$$\mathcal{H}(\bar{\boldsymbol{y}}, \boldsymbol{y}, \bar{\boldsymbol{z}}, \boldsymbol{z}) \le \max\{\mathcal{H}(\bar{\boldsymbol{y}}, \boldsymbol{y}, \bar{\boldsymbol{y}}, \boldsymbol{y}), \mathcal{H}(\bar{\boldsymbol{z}}, \boldsymbol{z}, \bar{\boldsymbol{z}}, \boldsymbol{z})\} \quad \forall \boldsymbol{y}, \boldsymbol{z} \in \mathbb{C}^N.$$

Proof: See Appendix F. ∎

In light of Theorem 3.5, one may ask whether we can find a λ large enough such that the conjugate-partial-symmetric fourth order tensor form $\mathcal{H}^\lambda$ associated with $\lambda(\boldsymbol{s}^\dagger \boldsymbol{s})^2 - f(\boldsymbol{s})$ satisfies (25). Unfortunately, this is not possible. In fact, let us consider the conjugate-partial-symmetric form $\mathcal{H}$ corresponding to the quartic function $(\boldsymbol{s}^\dagger \boldsymbol{s})^2$; then

$$\mathcal{H}(\boldsymbol{s}, \boldsymbol{y}, \boldsymbol{z}, \boldsymbol{w}) = \frac{1}{2}\left((\boldsymbol{s}^T \boldsymbol{y})(\boldsymbol{z}^T \boldsymbol{w}) + (\boldsymbol{z}^T \boldsymbol{y})(\boldsymbol{s}^T \boldsymbol{w})\right).$$

Thus, $\mathcal{H}(\bar{\boldsymbol{y}}, \boldsymbol{y}, \bar{\boldsymbol{z}}, \boldsymbol{z}) = \frac{1}{2}((\boldsymbol{y}^\dagger \boldsymbol{y})(\boldsymbol{z}^\dagger \boldsymbol{z}) + (\boldsymbol{z}^\dagger \boldsymbol{y})(\boldsymbol{y}^\dagger \boldsymbol{z}))$, $\mathcal{H}(\bar{\boldsymbol{z}}, \boldsymbol{y}, \bar{\boldsymbol{z}}, \boldsymbol{y}) = (\boldsymbol{z}^\dagger \boldsymbol{y})(\boldsymbol{z}^\dagger \boldsymbol{y})$, and $\mathcal{H}(\bar{\boldsymbol{y}}, \boldsymbol{z}, \bar{\boldsymbol{y}}, \boldsymbol{z}) = (\boldsymbol{y}^\dagger \boldsymbol{z})(\boldsymbol{y}^\dagger \boldsymbol{z})$. Moreover,

$$2\mathcal{H}(\bar{\boldsymbol{y}}, \boldsymbol{y}, \bar{\boldsymbol{z}}, \boldsymbol{z}) + \mathcal{H}(\bar{\boldsymbol{y}}, \boldsymbol{z}, \bar{\boldsymbol{y}}, \boldsymbol{z}) + \mathcal{H}(\bar{\boldsymbol{z}}, \boldsymbol{y}, \bar{\boldsymbol{z}}, \boldsymbol{y}) = \boldsymbol{y}^\dagger \boldsymbol{y} \boldsymbol{z}^\dagger \boldsymbol{z} + \boldsymbol{y}^\dagger \boldsymbol{z} \boldsymbol{z}^\dagger \boldsymbol{y} + \boldsymbol{y}^\dagger \boldsymbol{z} \boldsymbol{y}^\dagger \boldsymbol{z} + \boldsymbol{z}^\dagger \boldsymbol{y} \boldsymbol{z}^\dagger \boldsymbol{y}.$$

Simply choosing $\boldsymbol{y} = j\boldsymbol{z}$ leads to $2\mathcal{H}(\bar{\boldsymbol{y}}, \boldsymbol{y}, \bar{\boldsymbol{z}}, \boldsymbol{z}) + \mathcal{H}(\bar{\boldsymbol{y}}, \boldsymbol{z}, \bar{\boldsymbol{y}}, \boldsymbol{z}) + \mathcal{H}(\bar{\boldsymbol{z}}, \boldsymbol{y}, \bar{\boldsymbol{z}}, \boldsymbol{y}) = 0$ implying that it is not strictly positive, so the technique in Corollary 3.4 cannot be applied here.

This phenomenon lies in the fact that (25) is a stronger condition than the convexity requirements (20). To see this, let us consider a complex quartic function whose associated conjugate-partial-symmetric tensor $\mathcal{H}$ satisfies (25); then

$$2\mathcal{H}(\bar{\boldsymbol{y}}, \boldsymbol{y}, \bar{\boldsymbol{z}}, \boldsymbol{z}) \ge -\mathcal{H}(\bar{\boldsymbol{y}}, \boldsymbol{z}, \bar{\boldsymbol{y}}, \boldsymbol{z}) - \mathcal{H}(\bar{\boldsymbol{z}}, \boldsymbol{y}, \bar{\boldsymbol{z}}, \boldsymbol{y}), \quad \forall \boldsymbol{y}, \boldsymbol{z} \in \mathbb{C}^N,$$

and replacing $\boldsymbol{y}$ by $e^{j\theta}\boldsymbol{y}$, we have

$$\begin{aligned} 2\mathcal{H}(\bar{\boldsymbol{y}}, \boldsymbol{y}, \bar{\boldsymbol{z}}, \boldsymbol{z}) &= 2\mathcal{H}(\overline{e^{j\theta}\boldsymbol{y}}, e^{j\theta}\boldsymbol{y}, \bar{\boldsymbol{z}}, \boldsymbol{z}) \\ &\ge -\mathcal{H}(\overline{e^{j\theta}\boldsymbol{y}}, \boldsymbol{z}, \overline{e^{j\theta}\boldsymbol{y}}, \boldsymbol{z}) - \mathcal{H}(\bar{\boldsymbol{z}}, e^{j\theta}\boldsymbol{y}, \bar{\boldsymbol{z}}, e^{j\theta}\boldsymbol{y}) \\ &= -2\Re\left(e^{j2\theta}\mathcal{H}(\bar{\boldsymbol{z}}, \boldsymbol{y}, \bar{\boldsymbol{z}}, \boldsymbol{y})\right), \\ &\qquad \forall \boldsymbol{y}, \boldsymbol{z} \in \mathbb{C}^N,\ \theta \in [0, 2\pi]. \end{aligned}$$

Obviously, choosing

$$2\theta = \pi - \arg\left(\mathcal{H}(\bar{\boldsymbol{z}}, \boldsymbol{y}, \bar{\boldsymbol{z}}, \boldsymbol{y})\right),$$

it holds that $\mathcal{H}(\bar{\boldsymbol{y}}, \boldsymbol{y}, \bar{\boldsymbol{z}}, \boldsymbol{z}) \ge 0 \quad \forall \boldsymbol{y}, \boldsymbol{z} \in \mathbb{C}^N$. Now adding $2\mathcal{H}(\bar{\boldsymbol{y}}, \boldsymbol{y}, \bar{\boldsymbol{z}}, \boldsymbol{z})$ to the left hand side of (25), we have that $\forall \boldsymbol{y}, \boldsymbol{z} \in \mathbb{C}^N$

$$\begin{aligned} &4\mathcal{H}(\bar{\boldsymbol{y}}, \boldsymbol{y}, \bar{\boldsymbol{z}}, \boldsymbol{z}) + \mathcal{H}(\bar{\boldsymbol{y}}, \boldsymbol{z}, \bar{\boldsymbol{y}}, \boldsymbol{z}) + \mathcal{H}(\bar{\boldsymbol{z}}, \boldsymbol{y}, \bar{\boldsymbol{z}}, \boldsymbol{y}) \\ &\quad \ge 2\mathcal{H}(\bar{\boldsymbol{y}}, \boldsymbol{y}, \bar{\boldsymbol{z}}, \boldsymbol{z}) + \mathcal{H}(\bar{\boldsymbol{y}}, \boldsymbol{z}, \bar{\boldsymbol{y}}, \boldsymbol{z}) + \mathcal{H}(\bar{\boldsymbol{z}}, \boldsymbol{y}, \bar{\boldsymbol{z}}, \boldsymbol{y}) \ge 0, \end{aligned}$$

implying that the corresponding complex quartic function is convex. However, since the difference between (25) and (20) is very subtle, in practice we decide to use the same λ both in

Algorithm MBIL and in **Algorithm MBIQ**. Some useful remarks on **Algorithm MBIQ** are now given:

i) Due to Proposition A.1, in Appendix A-2, $\boldsymbol{B}^1$ and $\boldsymbol{B}^2$ in step 1 are Hermitian matrices.
ii) The complex quadratic problems in step 1 are still NP-hard; in practice we apply the randomization algorithms in [27] to get a good approximate solution.
iii) In order to improve the quality of the solution, we could repeatedly use the MBIQ approach, setting $\boldsymbol{s}_0^1 = \boldsymbol{s}_0^2 = \boldsymbol{s}_{k+1}^{n^*}$ as new starting points, if further progress is still possible.

Finally, the third proposed algorithm exploits both the conjugate-partial-symmetric tensor representation and the conjugate-super-symmetric tensor representation of the complex quartic functions. Namely, let $\mathcal{H}^\lambda$ and $\mathcal{G}^\lambda$ be the conjugate-partial-symmetric tensor form and conjugate-super-symmetric tensor form such that (24) and (18) are respectively satisfied. Then, we introduce an MBI type method for problem $\widetilde{\mathrm{CQ}}_\lambda^\infty$ (resp. $\widetilde{\mathrm{CQ}}_\lambda^M$) which resorts to a quadratic-improvement subroutine for at most K iterations and then switches to a linear-improvement subroutine, as described in **Algorithm MBIQ&L**. Otherwise stated, it exploits **Algorithm MBIL** starting from a good initial point, which is obtained through **Algorithm MBIQ**.

Algorithm MBIQ&L: MBI method with a quadratic-improvement subroutine and a linear-improvement subroutine for $\widetilde{\mathrm{CQ}}_\lambda^\infty$ (resp. $\widetilde{\mathrm{CQ}}_\lambda^M$)

0 (Initialization): Generate, possibly randomly, $(\boldsymbol{s}_0^1, \boldsymbol{s}_0^2)$ with $s_0^m \in \Omega^\infty$ (resp. Ω^M) for $m = 1, 2$ and compute the initial objective value $v_0 = \mathcal{H}^\lambda(\bar{\boldsymbol{s}}_0^1, \boldsymbol{s}_0^1, \bar{\boldsymbol{s}}_0^2, \boldsymbol{s}_0^2)$. Set $k = 0$.

1 (Block Quadratic Improvement): Let

$$\boldsymbol{B}^1 \to \mathcal{H}^\lambda(\cdot, \cdot, \bar{\boldsymbol{s}}_k^2, \boldsymbol{s}_k^2),\ \boldsymbol{B}^2 \to \mathcal{H}^\lambda(\bar{\boldsymbol{s}}_k^1, \boldsymbol{s}_k^1, \cdot, \cdot),$$

be the matrices associated with the bilinear functions on the right side.

For $m = 1, 2$ let

$$\boldsymbol{y}_{k+1}^m = \arg\max_{\boldsymbol{s}\in\Omega_\infty} (\boldsymbol{s})^\dagger \boldsymbol{B}^m \boldsymbol{s} \text{ (resp. } \boldsymbol{y}_{k+1}^m = \arg\max_{\boldsymbol{s}\in\Omega_M} (\boldsymbol{s})^\dagger \boldsymbol{B}^m \boldsymbol{s}),\ w_{k+1}^m = (\boldsymbol{y}_{k+1}^m)^\dagger \boldsymbol{B}^m \boldsymbol{y}_{k+1}^m.$$

2 (Maximum Improvement): Let $w_{k+1} = \max_{1\le m\le 2} w_{k+1}^m$ and $m^* = \arg\max_{1\le m\le 2} w_{k+1}^m$. Replace $\boldsymbol{s}_{k+1}^m = \boldsymbol{s}_k^m$ for all $m \neq m^*$, $\boldsymbol{s}_{k+1}^{m^*} = \boldsymbol{y}_{k+1}^{m^*}$ and $v_{k+1} = w_{k+1}$.

3 (Switch Condition): Set $k = k + 1$. If $|\frac{v_{k+1}-v_k}{\max(1,v_k)}| < \epsilon$ or $k = K$, set $\boldsymbol{s}_{K+1}^1 = \boldsymbol{s}_{K+1}^3 = \boldsymbol{s}_K^1$, $\boldsymbol{s}_{K+1}^2 = \boldsymbol{s}_{K+1}^4 = \boldsymbol{s}_K^2$, $v_{K+1} = \mathcal{G}^\lambda((\frac{\boldsymbol{s}_{K+1}^1}{\bar{\boldsymbol{s}}_{K+1}^1}), (\frac{\boldsymbol{s}_{K+1}^2}{\bar{\boldsymbol{s}}_{K+1}^2}), (\frac{\boldsymbol{s}_{K+1}^3}{\bar{\boldsymbol{s}}_{K+1}^3}), (\frac{\boldsymbol{s}_{K+1}^4}{\bar{\boldsymbol{s}}_{K+1}^4}))$ and go to step 4. Otherwise go to step 1.

4 (Block Linear Improvement): Let

$$\boldsymbol{c}^1 \to \mathcal{G}^\lambda(\cdot, (\tfrac{\boldsymbol{s}_k^2}{\bar{\boldsymbol{s}}_k^2}), (\tfrac{\boldsymbol{s}_k^3}{\bar{\boldsymbol{s}}_k^3}), (\tfrac{\boldsymbol{s}_k^4}{\bar{\boldsymbol{s}}_k^4})),\ \boldsymbol{c}^2 \to \mathcal{G}^\lambda((\tfrac{\boldsymbol{s}_k^1}{\bar{\boldsymbol{s}}_k^1}), \cdot, (\tfrac{\boldsymbol{s}_k^3}{\bar{\boldsymbol{s}}_k^3}), (\tfrac{\boldsymbol{s}_k^4}{\bar{\boldsymbol{s}}_k^4})),$$

$$\boldsymbol{c}^3 \to \mathcal{G}^\lambda((\tfrac{\boldsymbol{s}_k^1}{\bar{\boldsymbol{s}}_k^1}), (\tfrac{\boldsymbol{s}_k^2}{\bar{\boldsymbol{s}}_k^2}), \cdot, (\tfrac{\boldsymbol{s}_k^4}{\bar{\boldsymbol{s}}_k^4})),\ \boldsymbol{c}^4 \to \mathcal{G}^\lambda((\tfrac{\boldsymbol{s}_k^1}{\bar{\boldsymbol{s}}_k^1}), (\tfrac{\boldsymbol{s}_k^1}{\bar{\boldsymbol{s}}_k^1}), (\tfrac{\boldsymbol{s}_k^3}{\bar{\boldsymbol{s}}_k^3}), \cdot),$$

be the vectors associated with the linear functions on the right side.

For $m = 1, 2, 3, 4$ let

$$\boldsymbol{y}_{k+1}^m = \arg\max_{\boldsymbol{s}\in\Omega_\infty} (\tfrac{\boldsymbol{s}}{\bar{\boldsymbol{s}}})^T \boldsymbol{c}^m \text{ (resp. } \arg\max_{\boldsymbol{s}\in\Omega_M} (\tfrac{\boldsymbol{s}}{\bar{\boldsymbol{s}}})^T \boldsymbol{c}^m),\ w_{k+1}^m = (\tfrac{\boldsymbol{y}_{k+1}^m}{\bar{\boldsymbol{y}}_{k+1}^m})^T \boldsymbol{c}^m.$$

5 (Maximum Improvement): Let $w_{k+1} = \max_{1\le m\le 4} w_{k+1}^m$ and $m^* = \arg\max_{1\le m\le 4} w_{k+1}^m$. Replace $\boldsymbol{s}_{k+1}^m = \boldsymbol{s}_k^m$ for all $m \neq m^*$, $\boldsymbol{s}_{k+1}^{m^*} = \boldsymbol{y}_{k+1}^{m^*}$ and $v_{k+1} = w_{k+1}$.

6 (Stopping Criterion): If $|\frac{v_{k+1}-v_k}{\max(1,v_k)}| < \epsilon$, stop. Otherwise, set $k = k + 1$, and go to step 1.

7 (Output): For $1 \le n \le 4$, let

$$t^n = \mathcal{G}^\lambda((\tfrac{\boldsymbol{s}_{k+1}^n}{\bar{\boldsymbol{s}}_{k+1}^n}), (\tfrac{\boldsymbol{s}_{k+1}^n}{\bar{\boldsymbol{s}}_{k+1}^n}), (\tfrac{\boldsymbol{s}_{k+1}^n}{\bar{\boldsymbol{s}}_{k+1}^n}), (\tfrac{\boldsymbol{s}_{k+1}^n}{\bar{\boldsymbol{s}}_{k+1}^n})),$$

$n^* = \arg\max_{1\le n\le 4} t^n$. Return t^{n^*} and $\boldsymbol{s}_{k+1}^{n^*}$.

Computational Complexity Issues: It depends on the number of iterations $\overline{N}$ as well as on the complexity involved in each iteration. Precisely, we have:

- **Algorithm MBIL**: the overall complexity is linear with respect to $\overline{N}$ (see Appendix G for the local convergence analysis) and, in each iteration, it includes the computation of the vectors $\boldsymbol{c}^i, i = 1, 2, 3, 4$, the solutions to the block linear improvement problems, and the maximum improvement. As to the computation of the vectors $\boldsymbol{c}^i, i = 1, 2, 3, 4$, the complexity is linear with respect to N; moreover the optimal solution to each linear block improvement problem is computed in closed form when $\boldsymbol{s} \in \Omega^\infty$ and can be obtained with a linear complexity with respect to N when $\boldsymbol{s} \in \Omega^M$.
- **Algorithm MBIQ**: the overall complexity is linear with respect to $\overline{N}$ (see Appendix G for the local convergence analysis) and, in each iteration, it includes the computation of the matrices $\boldsymbol{B}^i, i = 1, 2$, the solutions to the quadratic block improvement problems, and the maximum improvement. As to the computation of the matrices $\boldsymbol{B}^i, i = 1, 2$, the complexity is quadratic with respect to N; moreover, a good approximate solution to each quadratic block improvement problem, is computed resorting to the randomization algorithms in [27], whose complexity is $O(N^{3.5}\log(1/\eta))$, where η is a prescribed accuracy, for a moderate number of randomizations.
- **Algorithm MBIQ&L**: the overall complexity can be obtained by combining the complexity associated with the $\overline{K} \le K$ iterations of **Algorithm MBIQ** and the $\overline{N} - \overline{K}$ iterations of **Algorithm MBIL**.

Summary. We have formulated the problem of minimizing the average value of the ambiguity function of the transmitted phase-only signal over some range-Doppler bins via optimization problem P^∞ (resp. P^M for the quantized case). We have proved that P^∞ (resp. P^M) belongs to the general class of complex quartic minimization problems CQ^∞ (resp. CQ^M). Exploiting the equivalence among problem CQ^∞ (resp. CQ^M) and problem $\widetilde{\mathrm{CQ}}_\lambda^\infty$ (resp. $\widetilde{\mathrm{CQ}}_\lambda^M$) for any the real value of the

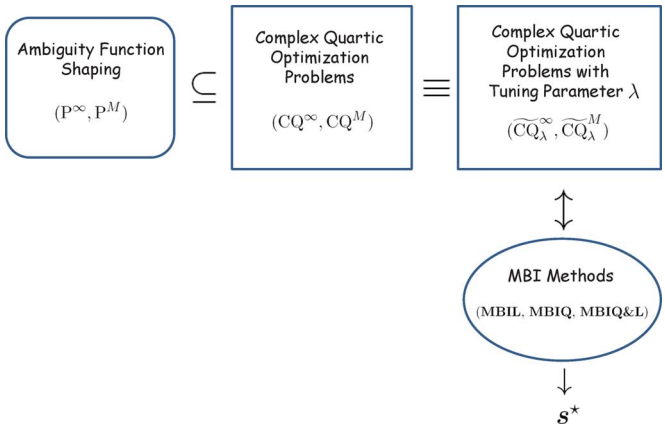

Fig. 2. A pictorial representation of the steps involved in definition of the MBI methods.

tuning parameter λ, we have devised optimization techniques based on the MBI approach to get good quality solutions to problem CQ^{∞} (resp. CQ^{M}). Interestingly, an appropriate selection of λ enforces important properties to the devised optimization methods (see Corollary 3.4 and Theorem 3.2). Fig. 2 shows a pictorial representation of the relationships among the optimization problems involved in the design of the proposed MBI optimization procedures.

IV. Performance Assessment

In this section, we analyze the capability of the proposed MBI type algorithms to select a radar phase code with a properly shaped ambiguity function. Precisely, we focus on the design of a continuous phase code exploiting the following three-step based procedure:

1) select the value of the parameter $\lambda > 0$, denoted by $\tilde{\lambda}$, for instance such that $\tilde{\lambda}(\boldsymbol{s}^{\dagger}\boldsymbol{s})^2 - \phi(\boldsymbol{s})$ is convex;
2) starting from K_1 different initial points, apply **Algorithm MBIL**, **Algorithm MBIQ**, and **Algorithm MBIQ&L** to problem $\widetilde{\mathrm{CQ}}_{\tilde{\lambda}}^{\infty}$ with $f(\boldsymbol{s}) = \phi(\boldsymbol{s})$;
3) get a feasible point $\boldsymbol{s}^{\star}$ for P^{∞}, picking the solution which leads to the minimum objective function among the outputs of the three algorithms.

As to the parameter λ, Corollary 3.4 provides a systematic approach to compute it in order to ensure the convexity of the objective function $\tilde{\lambda}(\boldsymbol{s}^{\dagger}\boldsymbol{s})^2 - \phi(\boldsymbol{s})$; by doing so, the monotonicity of **Algorithm MBIL** is guaranteed by Theorem 3.2 and the monotonicity of **Algorithm MBIQ** is expected from Theorem 3.5. Nevertheless, if $\tilde{\lambda}$ is too high, the original objective function $-\phi(\boldsymbol{s})$ is significantly changed with respect to the one considered in the MBI type algorithms and the numerical performance of the proposed procedures could be consequently affected (the bias term $\tilde{\lambda}N^2$ could mask, from a numerical point of view, the variations in the objective function $\phi(\boldsymbol{s})$). Additionally, it is worth observing that our procedures do not work directly on $\tilde{\lambda}(\boldsymbol{s}^{\dagger}\boldsymbol{s})^2 - \phi(\boldsymbol{s})$. For instance, let us consider **Algorithm MBIQ** and investigate the biquadratic function associated with $\tilde{\lambda}(\boldsymbol{s}^{\dagger}\boldsymbol{s})^2$ in each subproblem. Let $\mathcal{H}_1$ be the conjugate-partial-symmetric tensor associated with $\tilde{\lambda}(\boldsymbol{s}^{\dagger}\boldsymbol{s})^2$; then the multi-linear function induced by $\mathcal{H}_1$ is

$$\mathcal{H}_1(\boldsymbol{s},\boldsymbol{y},\boldsymbol{z},\boldsymbol{w}) = \frac{\tilde{\lambda}}{2}\left((\boldsymbol{s}^T\boldsymbol{y})(\boldsymbol{z}^T\boldsymbol{w}) + (\boldsymbol{z}^T\boldsymbol{y})(\boldsymbol{s}^T\boldsymbol{w})\right).$$

Letting $\boldsymbol{s} = \bar{\boldsymbol{y}}$ and $\boldsymbol{z} = \bar{\boldsymbol{w}}$, we get the biquadratic function in the subproblems

$$\mathcal{H}_1(\bar{\boldsymbol{y}},\boldsymbol{y},\bar{\boldsymbol{w}},\boldsymbol{w}) = \frac{\tilde{\lambda}}{2}\left((\boldsymbol{y}^{\dagger}\boldsymbol{y})(\boldsymbol{w}^{\dagger}\boldsymbol{w}) + (\boldsymbol{w}^{\dagger}\boldsymbol{y})(\boldsymbol{y}^{\dagger}\boldsymbol{w})\right).$$

Notice that for any vectors $\boldsymbol{y},\boldsymbol{w} \in \Omega_{\infty}$, $\boldsymbol{w} = \arg\max_{\boldsymbol{z}\in\Omega_{\infty}} \mathcal{H}_1(\bar{\boldsymbol{z}},\boldsymbol{z},\bar{\boldsymbol{w}},\boldsymbol{w})$ and $\boldsymbol{y} = \arg\max_{\boldsymbol{z}\in\Omega_{\infty}} \mathcal{H}_1(\bar{\boldsymbol{y}},\boldsymbol{y},\bar{\boldsymbol{z}},\boldsymbol{z})$. Therefore, **Algorithm MBIQ** will terminate in one iteration if applied to $\mathcal{H}_1(\bar{\boldsymbol{y}},\boldsymbol{y},\bar{\boldsymbol{w}},\boldsymbol{w})$ and every $\boldsymbol{y} = \boldsymbol{w} \in \Omega_{\infty}$ is a global maximizer. As $\tilde{\lambda}$ increases, $\tilde{\lambda}(\boldsymbol{s}^{\dagger}\boldsymbol{s})^2$ will gradually dominate the whole function $\tilde{\lambda}(\boldsymbol{s}^{\dagger}\boldsymbol{s})^2 - \phi(\boldsymbol{s})$. Consequently, the local maxima of the relaxed function associated with $\tilde{\lambda}(\boldsymbol{s}^{\dagger}\boldsymbol{s})^2 - \phi(\boldsymbol{s})$ will be expected to gradually become that of the relaxed function associated with $\tilde{\lambda}(\boldsymbol{s}^{\dagger}\boldsymbol{s})^2$, thus increasing the probability of ending up in a low quality solution. Based on the previous considerations, a reasonable choice is to consider the smallest $\tilde{\lambda}$ ensuring the convexity. For this reason, denoting by $\lambda_1 = \frac{\lambda^{\star}}{2}$ with $\lambda^{\star}$ defined in (23), the focus will be on $\tilde{\lambda} \in \{\lambda_1, \lambda_1/3, \lambda_1/6\}$.

We conduct the performance analysis considering the two range-Doppler interference scenarios reported in Fig. 3, which are referred to as scenario 1 and scenario 2, respectively. In these interference maps, the red portions correspond to the regions of the unwanted range-Doppler returns (interference). In both scenarios, we discretize the normalized Doppler frequency axis into $N_{\nu} = 50$ bins, namely the discrete Doppler frequencies are $\nu_h = -\frac{1}{2} + h\frac{1}{50}, h = 0, 1, \ldots, 49$. Furthermore, we assume a uniform interference power among the interference bins. Precisely, in scenario 1 we suppose

$$p_{(r,h)} = \begin{cases} 1 & (r,h) \in \{2,3,4\} \times \{35,36,37,38\} \\ 1 & (r,h) \in \{3,4\} \times \{18,19,20\} \\ 0 & \text{otherwise} \end{cases},$$

whereas in scenario 2

$$p_{r,h} = \begin{cases} 1 & (r,h) \in \{2,3,4\} \times \{35,36,37,38\} \\ 1 & (r,h) \in \{3,4\} \times \{18,19,20\} \\ 1 & (r,h) \in \{1,2,\ldots,10\} \times \{25\} \\ 0 & \text{otherwise} \end{cases}.$$

Thus, in scenario 2 we also try to control the ISL over the first ten lags of the transmitted waveform. This can be of paramount importance in remote sensing applications where many scatterers share the same Doppler frequency of the patch of interest (distributed targets), as well as in a fast-time code design. Notice also that, due to the radar range equation, after a certain distance (corresponding to a certain discrete lag) the radar returns can be totally neglected and further constraints on the ambiguity function sidelobes become useless.

As to the parameters of the devised MBI type algorithms, we require a minimum iteration gain of $\epsilon = 10^{-6}$, and allow for a maximum value of 5000 iterations for **Algorithm MBIL**, and 200 iterations for **Algorithm MBIQ**. Additionally, as to the quadratic-improvement subroutine, involved in **Algorithm MBIQ** and **Algorithm MBIQ&L**, we assume that 100 randomizations are performed to get a good approximate solution. With reference to **Algorithm MBIQ&L**, we start from the same initial points used for **Algorithm MBIQ**; moreover, we execute the quadratic subroutine for at most $K = 10$ times and allow for at most 5000 runs of the linear subroutine.

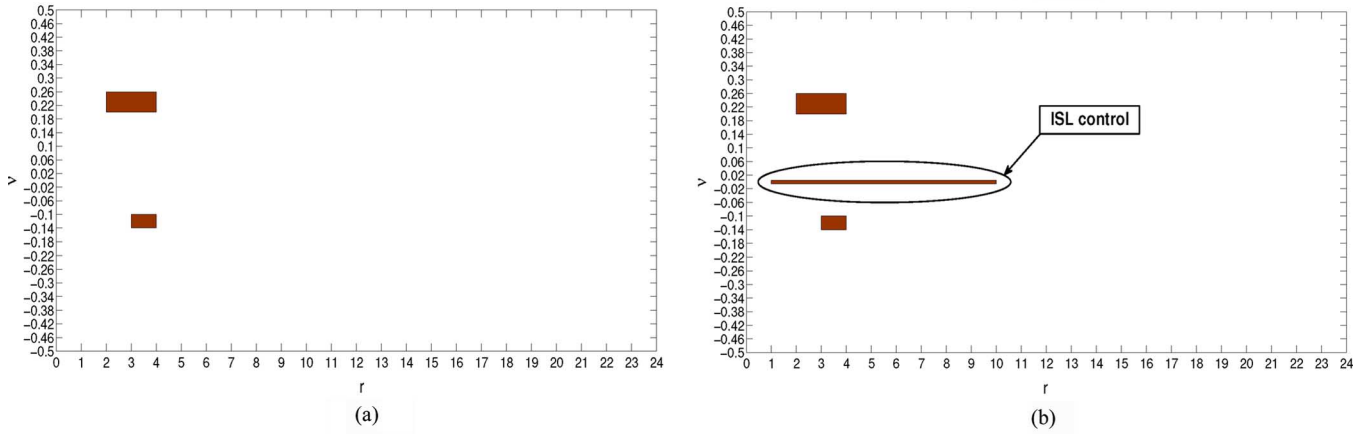

Fig. 3. (a) Range-Doppler inference map, scenario 1. (b) Range-Doppler inference map with ISL control, scenario 2.

In order to assess the performance of the proposed three-step based procedure for the design of a continuous phase code, we set $K_1 = 11$; specifically, in step 2 we run ten times the MBI type algorithms with independent random initial points[10], as well as once with the uncoded sequence[11] $\tilde{\boldsymbol{s}}$, $\tilde{s}(i) = 1,\ i = 1, 2, \ldots, N$; the best solution is kept as the devised code. The same initial points are used for any tested $\tilde{\lambda} \in \{\lambda_1, \lambda_1/3, \lambda_1/6\}$.

In Fig. 4, considering the interference scenario 1, we plot the Signal to Interference Ratio (SIR), defined as

$$\mathrm{SIR} = \frac{N^2}{\sum_{r=1}^{N}\sum_{h=1}^{N_\nu} p_{(r,h)} \|\boldsymbol{s}\|^2 \mathrm{g}_{\boldsymbol{s}}(r, \nu_h)},$$

versus the length of the code, averaged over 20 independent trials, for the codes $\boldsymbol{s}^\star_{\tilde{\lambda}_1}, \boldsymbol{s}^\star_{\tilde{\lambda}_1/3}, \boldsymbol{s}^\star_{\tilde{\lambda}_1/6}$ and the uncoded sequence $\tilde{\boldsymbol{s}}$. Also, the SIR achieved by the best radar code $\boldsymbol{s}^\star$, among $\{\boldsymbol{s}^\star_{\tilde{\lambda}_1}, \boldsymbol{s}^\star_{\tilde{\lambda}_1/3}, \boldsymbol{s}^\star_{\tilde{\lambda}_1/6}\}$ in each trial, is plotted (the synthesized code). As expected, the synthesized code outperforms the uncoded transmission, showing the capability of the proposed algorithm to contrast and suppress the interfering returns. Furthermore, increasing N, smaller values of $\tilde{\lambda}$ allow to obtain better performances, thereby confirming the numerical problems that could affect the proposed procedures when high values of $\tilde{\lambda}N^2$ are considered. Nevertheless, the value $\tilde{\lambda} = \lambda_1/6$ produces the worst performances for $N = 5$; this could be due to the non-convexity of $\lambda_1/6(\boldsymbol{s}^\dagger\boldsymbol{s})^2 - \phi(\boldsymbol{s})$ for $N = 5$. Notice also that, the achieved SIR values improve as N increases in agreement with the higher degrees of freedom available at the design stage. For comparison purpose, in Fig. 4, we also report

- the SIR, averaged over 20 independent trials, associated with the waveforms obtained through the Newton-Raphson technique proposed[12] in [5];
- the SIR, for the interference scenario 1, of the mismatched filters[13] associated with a polyphase Barker and a P3 code, respectively, [1].

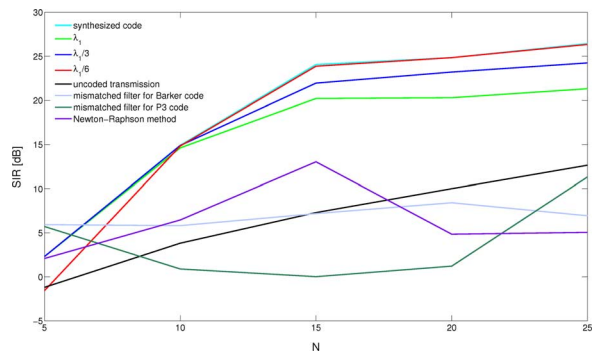

Fig. 4. SIR versus N, for the uncoded transmission, the synthesized code, the radar codes designed exploiting some $\tilde{\lambda}$ values, the code synthesized according to Newton-Raphson method [5], and the mismatched filters associated with a polyphase Barker and a P3 code, respectively.

The figure highlights that our design method can outperform that in [5]; furthermore, as N increases, the double suppression effect (both at transmission and at reception) connected with the proposed ambiguity function design, can lead to higher SIR values than those obtained through mismatched filters, which, on the other hand, do not account for dynamic range constraints on the filter coefficients.

In Fig. 5, we plot the ambiguity function contour map of the synthesized code for $N = 25$. Furthermore, in Figs. 6, we report the range-cut for different values of r (namely $r = [1, 2, 3, 4]$). These figures highlight the capability of the proposed algorithm to suitably shape the ambiguity function which presents deep nulls where interfering regions are foreseen.

In Fig. 7, we represent the square modulus of the autocorrelation function of the synthesized code for $N = 25$. Notice that, we have not imposed any constraints on the zero-Doppler cut of the ambiguity function; indeed, some sidelobe peaks can be observed in the plotted function. Finally, in Table I we

[10]Each point is a unimodular sequence with independent and identically distributed random phases, drawn by a uniform distribution over $[0, 2\pi]$.

[11]It is worth pointing out that other deterministic initial sequences could be considered.

[12]In each trial the algorithm is run twenty times with independent random initial points as well as once with the uncoded sequence. The algorithm terminates either when the norm of the gradient is less than 10^{-4} or when the number of iterations becomes greater than 200.

[13]We consider the interfering scenario 1 with a Clutter to Noise Ratio (CNR) equal to 40 dB. Besides, to allow for a fair comparison with the synthesized ambiguity function, we further assume the presence of $N-1$ fictitious interfering bin at range '0', with a CNR still equal to 40 dB.

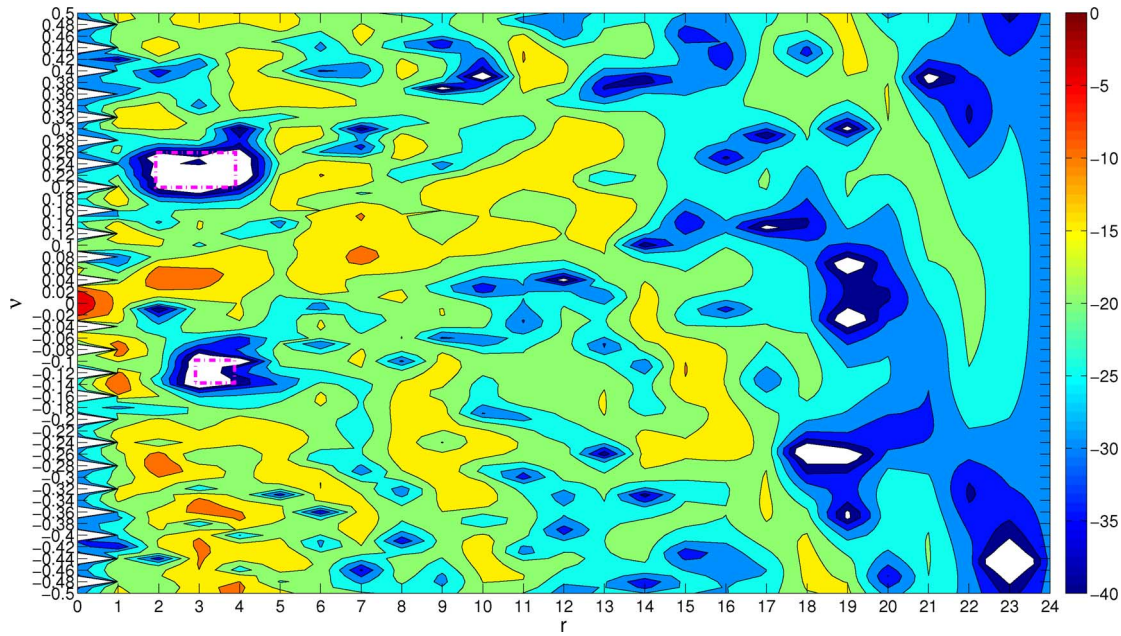

Fig. 5. Ambiguity function, in dB, of the synthesized code $\boldsymbol{s}^{\star}$ for $N = 25$ (also in fuchsia the assumed interfering regions).

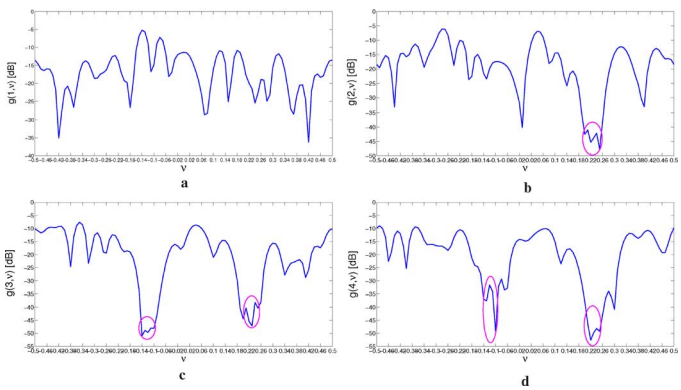

Fig. 6. (a) Ambiguity function cut at $r = 1$, in dB. (b) Ambiguity function cut at $r = 2$, in dB. (c) Ambiguity function cut at $r = 3$, in dB. (d) Ambiguity function cut at $r = 4$, in dB.

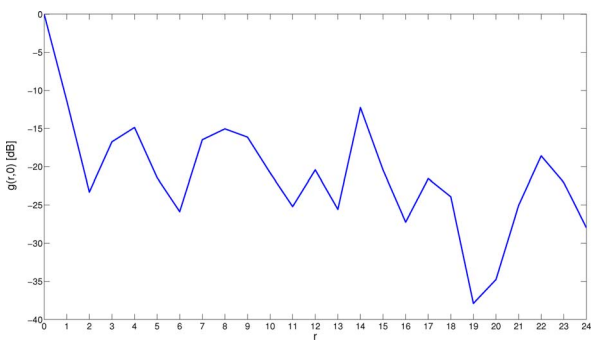

Fig. 7. Square modulus of the autocorrelation function, in dB, for $N = 25$.

present the average number of iterations (over 200 random initial points) of **Algorithm MBIL**, **Algorithm MBIQ**, and **Algorithm MBIQ&L**, for scenario 1. We can observe that the three proposed algorithms converge quite quickly, with a number of iterations usually less than 1000 for **Algorithm MBIL** and **Algorithm MBIQ&L**, and less than 200 for **Algorithm MBIQ**.

In Figs. 8, we plot the SIR versus the length of the code, for both the best radar code $\boldsymbol{s}^{\star}$ and the uncoded transmission $\tilde{\boldsymbol{s}}$, assuming the interference scenario 2. The SIRs achieved by the radar codes devised with the different $\tilde{\lambda}$ values are also reported. Again, an average value over 20 trials has been considered. In agreement with scenario 1, the synthesized code outperforms the uncoded transmission; besides, the curves obtained using the different values of $\tilde{\lambda}$, are much closer than those resulting from scenario 1. The figure also highlights that the achieved SIR improves as the code length N increases and this is due to the higher number of degrees of freedom available at the design stage. Additionally, it is interesting to note that the uncoded sequence achieves lower and lower SIR values as N increases, highlighting its incapability to contrast the foreseen unwanted returns and the need for a proper design of the transmitted radar code. As for scenario 1, in Fig. 8, we also report the SIR, averaged over 20 independent trials, of the waveforms devised according to the Newton-Raphson based technique proposed in [5]. Furthermore, we plot the SIR of the mismatched filters[14] associated with a polyphase Barker and a P3 code, respectively, [1]. Again our design method can outperform that in [5] and, for N greater than or equal to 10, a better interference suppression than the mismatched filters can be observed.

In Fig. 9, we report the ambiguity function contour map of the synthesized code for $N = 25$, while in Fig. 10, we show its range-cut, for different values of r ($r = [1, 2, 3, 4]$). As expected, the proposed algorithms suitably shape the range-Doppler response because the synthesized ambiguity function presents deep nulls where interfering regions are foreseen. Furthermore, the ambiguity function synthesized in scenario 1 presents lower values than the one synthesized in scenario 2 (compare Figs. 6 and 10) in the common range-Doppler interfering regions. This agrees with the fact

[14]We consider the interfering scenario 2 with a Clutter to Noise Ratio (CNR) equal to 40 dB. Besides, to allow for a fair comparison with the synthesized ambiguity function, we further assume the presence of $N - 1$ fictitious interfering bin at range '0', with a CNR still equal to 40 dB.

TABLE I
AVERAGE NUMBER OF ITERATIONS OF THE PROPOSED ALGORITHMS, FOR SCENARIO 1

N	λ_1				$\lambda_1/3$				$\lambda_1/6$			
	MBIL	MBIQ	MBIQ&L		MBIL	MBIQ	MBIQ&L		MBIL	MBIQ	MBIQ&L	
			Phase1	Phase2			Phase1	Phase2			Phase1	Phase2
5	79.64	27.41	10.00	53.68	38.62	13.16	9.95	12.73	40.77	15.95	9.92	50.46
10	484.72	150.43	10.00	414.74	321.73	115.63	10.00	322.37	247.60	31.67	10.00	178.41
15	739.99	192.87	10.00	725.50	669.33	172.58	10.00	600.66	499.64	113.04	10.00	472.05
20	671.98	195.95	10.00	673.08	710.99	189.94	10.00	659.23	667.88	174.45	10.00	652.44
25	666.74	196.05	10.00	583.48	646.73	194.00	10.00	628.88	700.93	189.89	10.00	637.31

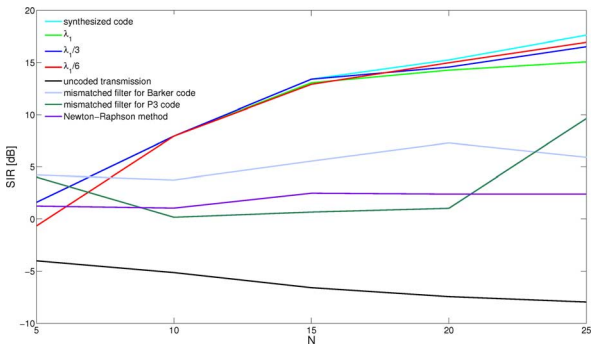

Fig. 8. SIR versus N, for the uncoded sequence, the synthesized code, the radar codes designed exploiting some $\tilde{\lambda}$ values, the code synthesized according to Newton-Raphson method [5], and the mismatched filters associated with a polyphase Barker and a P3 code, respectively.

that in scenario 2 an additional portion of the range-Doppler plane has to be controlled and the range-Doppler response is a continuous function sharing unitary volume, namely

$$\sum_{r=-N+1}^{N-1} \int_{-\frac{1}{2}}^{\frac{1}{2}} \mathrm{g}_{\boldsymbol{s}}(r,\nu) = 1,$$

with

$$\mathrm{g}_{\boldsymbol{s}}(r,\nu) = \mathrm{g}_{\boldsymbol{s}}(-r,-\nu).$$

Finally, in Fig. 11, we plot the square modulus of the autocorrelation function of the synthesized code, for $N = 25$. Thanks to the additional term in the objective which controls the ISL, the designed code also shares good autocorrelation properties in the time lags of interest. In Table II, we present the average number of iterations (over 200 random initial points) of **Algorithm MBIL**, **Algorithm MBIQ**, and **Algorithm MBIQ&L**, for scenario 2. We can observe that all the considered MBI type algorithms converge quite quickly, with a number of iterations usually less than 1000 for **Algorithm MBIL** and **Algorithm MBIQ&L**, and less than 200 for **Algorithm MBIQ**.

V. CONCLUSION

In this paper, we considered the problem of designing, in a cognitive way, a constant modulus waveform with a desired ambiguity function. Due to the hardness of the considered optimization problem, we focused on iterative techniques capable of providing, in polynomial time, good quality solutions. Precisely, we first devised MBI type optimization algorithms, based on linear- and quadratic-improvement subroutines. Then, we proposed an optimization procedure taking the best solution among those obtained through the aforementioned algorithms. At the analysis stage, we showed the capability of the proposed techniques to synthesize phase-only codes sharing the desired features in the ambiguity function shape, and, hence, the ability to effectively contrast the interfering returns.
Possible future research tracks might concern the development of an algorithm with a worst case performance guarantee as well as the design of a procedure ensuring the convergence to a Karush-Kuhn-Tucker (KKT) point.

APPENDIX

A. Complex Quartic Function and Associated Tensor Form

1) Complex Quartic Function: A real valued conjugate homogeneous quartic function, synthetically denoted in the following as complex quartic function, is defined as ([28], Proposition 4.3)

$$f(\boldsymbol{s}) = \sum_{\substack{1\le i\le k\le N\\ 1\le m\le \ell\le N}} b_{imk\ell}\bar{s}(i)s(m)\bar{s}(k)s(\ell), \tag{26}$$

where $\boldsymbol{s} \in \mathbb{C}^N$ and $b_{imk\ell} \in \mathbb{C}$, with $b_{imk\ell} = \bar{b}_{mi\ell k}$ for all $1 \le i \le k \le N$ and $1 \le m \le \ell \le N$. An equivalent form of (26), which is extensively used in this paper, is

$$f(\boldsymbol{s}) = \sum_{r_1=1}^{R_1} (\boldsymbol{s}^\dagger \boldsymbol{A}^{r_1}\boldsymbol{s})(\boldsymbol{s}^\dagger \boldsymbol{A}^{r_1\dagger}\boldsymbol{s}) - \sum_{r_1=R_1+1}^{R_2} (\boldsymbol{s}^\dagger \boldsymbol{A}^{r_1}\boldsymbol{s})(\boldsymbol{s}^\dagger \boldsymbol{A}^{r_1\dagger}\boldsymbol{s}) \tag{27}$$

$$= \sum_{imk\ell} \left(\sum_{r_1=1}^{R_1} A^{r_1}(i,m)\bar{A}^{r_1}(\ell,k) - \sum_{r_1=R_1+1}^{R_2} A^{r_1}(i,m)\bar{A}^{r_1}(\ell,k) \right) \bar{s}(i)s(m)\bar{s}(k)s(\ell) \tag{28}$$

$$= \sum_{\substack{1\le i\le k\le n\\ 1\le m\le \ell\le n}} b_{imk\ell}\bar{s}(i)s(m)\bar{s}(k)s(\ell), \tag{29}$$

where $\boldsymbol{A}^{r_1} \in \mathbb{C}^{N,N}$, $r_1 = 1, 2, \ldots, R_1, \ldots, R_2$ and

$$b_{imk\ell} = \sum_{(i',k')\in\Pi(i,k)} \sum_{(m',\ell')\in\Pi(m,\ell)} \left(\sum_{r_1=1}^{R_1} A^{r_1}(i',m')\bar{A}^{r_1}(\ell',k') - \sum_{r_1=R_1+1}^{R_2} A^{r_1}(i',m')\bar{A}^{r_1}(\ell',k') \right), \tag{30}$$

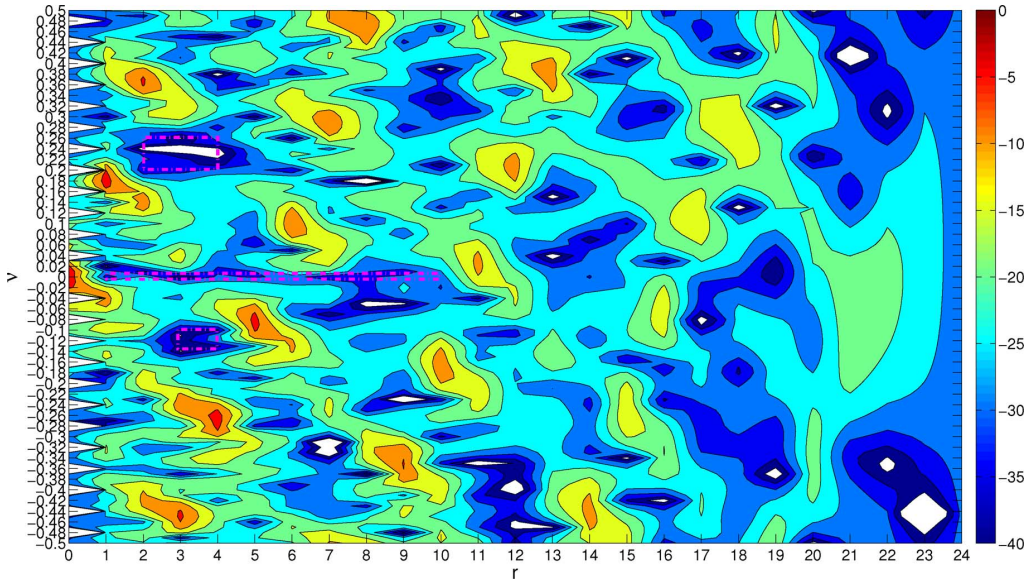

Fig. 9. Ambiguity function, in dB, of the synthesized transmission code $\boldsymbol{s}^\star$ for $N = 25$ (also in fuchsia the assumed interfering regions).

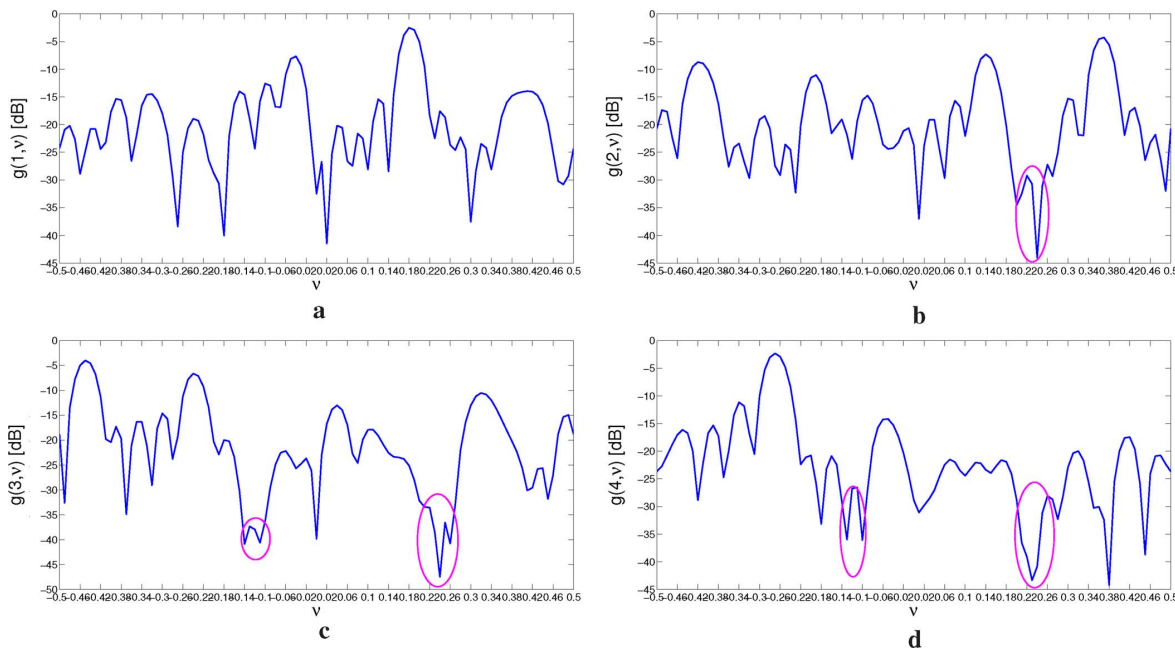

Fig. 10. (a) Ambiguity function cut at $r = 1$, in dB. (b) Ambiguity function cut at $r = 2$, in dB. (c) Ambiguity function cut at $r = 3$, in dB. (d) Ambiguity function cut at $r = 4$, in dB.

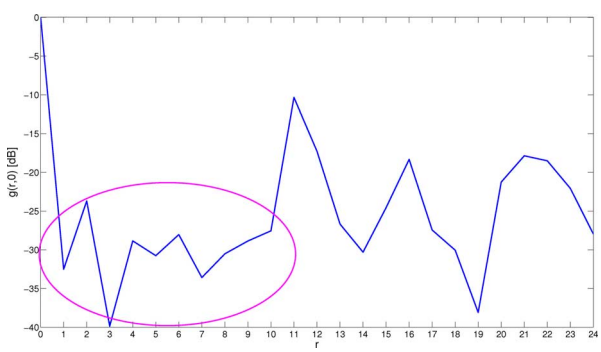

Fig. 11. Square modulus of the autocorrelation function, in dB, for $N = 25$.

with $\Pi(i,k)$ and $\Pi(m,\ell)$ the sets of all distinct permutations of the indices $\{i,k\}$ and $\{m,\ell\}$, respectively. Indeed, $A^{r_1}(i,m)\bar{A}^{r_1}(\ell,k) = \bar{A}^{r_1}(\ell,k)A^{r_1}(i,m) = \overline{A^{r_1}(\ell,k)\bar{A}^{r_1}(i,m)}$, for any 4-tuple (i,m,k,ℓ) and index r_1, thus by (30) $b_{imk\ell} = \bar{b}_{\ell kmi} = \bar{b}_{mi\ell k}$. Furthermore, any real valued complex quartic function can be expressed in the form (27).

Henceforth, we represent complex quartic functions by means of their corresponding tensor forms [28]–[30]. Suppose $\mathcal{F} = (\mathcal{F}_{imk\ell}) \in \mathbb{C}^{N,N,N,N}$ is a complex fourth order tensor, we define the following multi-linear function:

$$\mathcal{F}(\boldsymbol{s}^1,\boldsymbol{s}^2,\boldsymbol{s}^3,\boldsymbol{s}^4) = \sum_{imk\ell} \mathcal{F}_{imk\ell} s^1(i)s^2(m)s^3(k)s^4(\ell), \qquad (31)$$

where $\boldsymbol{s}^k \in \mathbb{C}^N$ for $k = 1,2,3,4$. If we further let $\boldsymbol{s}^1 = \boldsymbol{s}^3 = \bar{\boldsymbol{s}}$ and $\boldsymbol{s}^2 = \boldsymbol{s}^4 = \boldsymbol{s}$ in the above multi-linear function,

TABLE II
AVERAGE NUMBER OF ITERATIONS OF THE PROPOSED ALGORITHMS, FOR SCENARIO 2

N	λ_1				$\lambda_1/3$				$\lambda_1/6$			
	MBIL	MBIQ	MBIQ&L		MBIL	MBIQ	MBIQ&L		MBIL	MBIQ	MBIQ&L	
			Phase1	Phase2			Phase1	Phase2			Phase1	Phase2
5	84.35	26.57	10.00	50.59	38.10	12.14	9.91	11.03	40.36	16.05	9.90	55.46
10	528.20	148.45	10.00	481.06	250.34	88.77	10.00	210.88	166.29	51.09	9.98	127.47
15	713.01	181.44	10.00	669.18	448.10	130.16	10.00	387.18	259.24	76.83	10.00	221.54
20	814.18	191.44	10.00	824.97	567.61	162.88	10.00	567.55	403.44	124.66	10.00	377.17
25	892.01	197.10	10.00	849.51	693.44	184.38	10.00	688.79	556.53	164.81	10.00	536.50

then $\mathcal{F}_{imk\ell}, \mathcal{F}_{kmi\ell}, \mathcal{F}_{k\ell im}$ and $\mathcal{F}_{i\ell km}$ are the coefficients corresponding to the same monomial $\bar{s}(i)s(m)\bar{s}(k)s(\ell)$. To ensure

$$\mathcal{F}(\bar{\boldsymbol{s}}, \boldsymbol{s}, \bar{\boldsymbol{s}}, \boldsymbol{s}) = f(\boldsymbol{s}),$$

we need that, from ([28], Lemma 4.2),

$$\sum_{(i',k')\in\Pi(i,k)} \sum_{(m',\ell')\in\Pi(m,\ell)} \mathcal{F}_{i'm'k'\ell'} = b_{imk\ell}.$$

2) Conjugate-Partial-Symmetric Tensor Form: Based on the symmetry property shared by the Hermitian matrices characterizing bilinear forms, we would like the tensor form $\mathcal{F}$ to be symmetric in some sense.

Definition 1: We call a fourth order complex tensor $\mathcal{H} = (\mathcal{H}_{imk\ell})$ *conjugate-partial-symmetric*, if (i) $\mathcal{H}$ is partial-symmetric: $\mathcal{H}_{imk\ell} = \mathcal{H}_{kmi\ell} = \mathcal{H}_{k\ell im} = \mathcal{H}_{i\ell km}$ (ii) $\mathcal{H}_{imk\ell} = \bar{\mathcal{H}}_{mi\ell k}$ for any 4-tuple (i, m, k, ℓ).

The multi-linear function induced by the conjugate-partial-symmetric tensor $\mathcal{H}$ shares the following property.

Proposition A.1: Suppose $\mathcal{H}$ is a conjugate-partial-symmetric fourth order tensor; then for any $\boldsymbol{s}, \boldsymbol{y}, \boldsymbol{z}, \boldsymbol{w} \in \mathbb{C}^N$,

$$\mathcal{H}(\boldsymbol{s}, \boldsymbol{y}, \boldsymbol{z}, \boldsymbol{w}) = \mathcal{H}(\boldsymbol{z}, \boldsymbol{y}, \boldsymbol{s}, \boldsymbol{w}), = \mathcal{H}(\boldsymbol{z}, \boldsymbol{w}, \boldsymbol{s}, \boldsymbol{y}), = \mathcal{H}(\boldsymbol{s}, \boldsymbol{w}, \boldsymbol{z}, \boldsymbol{y}),$$
$$\text{and } \mathcal{H}(\boldsymbol{s}, \boldsymbol{y}, \boldsymbol{z}, \boldsymbol{w}) = \bar{\mathcal{H}}(\boldsymbol{y}, \boldsymbol{s}, \boldsymbol{w}, \boldsymbol{z}).$$

Notice that, for any complex quartic function $f(s)$, the conjugate-partial-symmetric tensor $\mathcal{H}$ given by

$$\mathcal{H}_{i'm'k'\ell'} = \frac{b_{imk\ell}}{Card\left(\Pi(i,k)\right) Card\left(\Pi(m,\ell)\right)} \quad \text{if } (i',k') \in \Pi(i,k) \text{ and } (m',\ell') \in \Pi(m,\ell), \tag{32}$$

is such that

$$f(\boldsymbol{s}) = \mathcal{H}(\bar{\boldsymbol{s}}, \boldsymbol{s}, \bar{\boldsymbol{s}}, \boldsymbol{s}).$$

Otherwise stated, based on (32), any complex quartic function $f(\boldsymbol{s})$ uniquely determines a conjugate-partial-symmetric tensor $\mathcal{H} = (\mathcal{H}_{imk\ell})$ and vice versa.

3) Conjugate-Super-Symmetric Tensor Form: In this subsection we introduce a stronger symmetry feature than the conjugate-partial-symmetry; it plays an important role in this paper.

Definition 2: We call a fourth order complex tensor $\mathcal{G} = (\mathcal{G}_{imk\ell})$ *conjugate-super-symmetric*, if (i) $\mathcal{G}$ is *super-symmetric*, namely

$$\mathcal{G}_\pi = \mathcal{G}_{imk\ell}, \text{ if } \pi \in \Pi(i,m,k,\ell),$$

where $\Pi(i,m,k,\ell)$ is the set of all distinct permutations of the indices $\{i,m,k,\ell\}$, (ii) $\mathcal{G}_{i^1i^2i^3i^4} = \bar{\mathcal{G}}_{j^1j^2j^3j^4}$ if $|i^k - j^k| = N$, for all $1 \le k \le 4$.

As a direct consequence of conjugate-super-symmetry, it holds that

$$\begin{aligned}
&\overline{\mathcal{G}\left(\begin{pmatrix}\boldsymbol{s}^1\\ \bar{\boldsymbol{s}}^1\end{pmatrix}, \begin{pmatrix}\boldsymbol{s}^2\\ \bar{\boldsymbol{s}}^2\end{pmatrix}, \begin{pmatrix}\boldsymbol{s}^3\\ \bar{\boldsymbol{s}}^3\end{pmatrix}, \begin{pmatrix}\boldsymbol{s}^4\\ \bar{\boldsymbol{s}}^4\end{pmatrix}\right)} \\
=&\bar{\mathcal{G}}\left(\begin{pmatrix}\bar{\boldsymbol{s}}^1\\ \boldsymbol{s}^1\end{pmatrix}, \begin{pmatrix}\bar{\boldsymbol{s}}^2\\ \boldsymbol{s}^2\end{pmatrix}, \begin{pmatrix}\bar{\boldsymbol{s}}^3\\ \boldsymbol{s}^3\end{pmatrix}, \begin{pmatrix}\bar{\boldsymbol{s}}^4\\ \boldsymbol{s}^4\end{pmatrix}\right) \\
=&\mathcal{G}\left(\begin{pmatrix}\boldsymbol{s}^1\\ \bar{\boldsymbol{s}}^1\end{pmatrix}, \begin{pmatrix}\boldsymbol{s}^2\\ \bar{\boldsymbol{s}}^2\end{pmatrix}, \begin{pmatrix}\boldsymbol{s}^3\\ \bar{\boldsymbol{s}}^3\end{pmatrix}, \begin{pmatrix}\boldsymbol{s}^4\\ \bar{\boldsymbol{s}}^4\end{pmatrix}\right),
\end{aligned} \tag{33}$$

which means that $\mathcal{G}(\binom{\boldsymbol{s}^1}{\bar{\boldsymbol{s}}^1}, \binom{\boldsymbol{s}^2}{\bar{\boldsymbol{s}}^2}, \binom{\boldsymbol{s}^3}{\bar{\boldsymbol{s}}^3}, \binom{\boldsymbol{s}^4}{\bar{\boldsymbol{s}}^4})$ is always real-valued.

Notice that, for any complex quartic function $f(s)$, the conjugate-super-symmetry tensor $\mathcal{G}$ given at the bottom of the page by (34) is such that

$$f(\boldsymbol{s}) = \mathcal{G}\left(\begin{pmatrix}\boldsymbol{s}\\ \bar{\boldsymbol{s}}\end{pmatrix}, \begin{pmatrix}\boldsymbol{s}\\ \bar{\boldsymbol{s}}\end{pmatrix}, \begin{pmatrix}\boldsymbol{s}\\ \bar{\boldsymbol{s}}\end{pmatrix}, \begin{pmatrix}\boldsymbol{s}\\ \bar{\boldsymbol{s}}\end{pmatrix}\right).$$

Otherwise stated, based on (34), any complex quartic function $f(\boldsymbol{s})$ uniquely determines a conjugate-super-symmetric tensor $\mathcal{G} = (\mathcal{G}_{imk\ell})$ and vice versa.

So far, we have established two alternative representations for the real valued conjugate homogeneous fourth order complex function $f(\boldsymbol{s})$ given in (26), or in (27), in terms of two different tensor forms, both of which will be frequently used in our analysis. The former representation makes use of a conjugate-partial-symmetric tensor $\mathcal{H} \in \mathbb{C}^{N,N,N,N}$ (defined via (32)), the latter exploits a conjugate-super-symmetric tensor

$$\begin{cases} \mathcal{G}_\pi = b_{imk\ell}/Card\left(\Pi(N+i,m,N+k,\ell)\right), & \text{if } \pi \in \Pi(N+i,m,N+k,\ell) \text{ with } (i,m,k,\ell) \in \{1,2,\ldots,N\}^4 \\ \mathcal{G}_\pi = 0, & \text{otherwise.} \end{cases} \tag{34}$$

$\mathcal{G} \in \mathbb{C}^{2N\times 2N\times 2N\times 2N}$ (defined via (34)). We point out that the conjugate-partial-symmetric tensor $\mathcal{H}$ lies in a smaller tensor space than the conjugate-super-symmetric tensor $\mathcal{G}$, even if $\mathcal{G}$ shares a nicer symmetry property than $\mathcal{H}$.

B. Proof of Theorem 3.1

Proof: Let us focus on problem CQ^{∞}, a similar proof holds true for problem CQ^{M}. We consider a reduction from a known NP-hard problem [27]:

$$\mathrm{P}\ \begin{cases} \min\limits_{\boldsymbol{y}} & \boldsymbol{y}^{\dagger}\boldsymbol{Q}\boldsymbol{y} \\ \text{s.t.} & y_i \in \Omega_{\infty},\ i=1,2,\ldots,N, \end{cases} \tag{35}$$

where $\boldsymbol{Q}$ is a complex Hermitian positive semidefinite matrix. Performing the variable transformation $y_i \mapsto (s_i)^2$, $i=1,2,\ldots,N$, and observing that $y_i \in \Omega_{\infty}$ if and only if $s_i \in \Omega_{\infty}$, problem P is equivalent to the following complex quartic problem:

$$\mathrm{P}_1\ \begin{cases} \min\limits_{\boldsymbol{s}} & \sum\limits_{\ell,h} Q_{\ell h}(\bar{s}_{\ell})^2(s_h)^2 \\ \text{s.t.} & s_i \in \Omega_{\infty},\ i=1,2,\ldots,N \end{cases}, \tag{36}$$

which can be written in the form of CQ^{∞} (11), since for any $1 \le h,k \le N$

$$\begin{aligned}\left(|Q_{kh}\bar{x}_k x_h + x_k\bar{x}_h|^2 - |Q_{hk}\bar{x}_h x_k - x_h\bar{x}_k|^2\right)/2 \\ = Q_{kh}(\bar{x}_k)^2(x_h)^2 + Q_{hk}(\bar{x}_h)^2(x_k)^2.\end{aligned}$$

Therefore, the conclusion immediately follows from the NP-hardness of problem P. ∎

C. Proof of Theorem 3.2

Proof: The key idea here is to apply inequality (21) twice. First of all denote $\boldsymbol{y}' = \boldsymbol{s}^1 + \boldsymbol{s}^2$, $\boldsymbol{y}'' = \boldsymbol{s}^1 - \boldsymbol{s}^2$, $\boldsymbol{z}' = \boldsymbol{s}^3 + \boldsymbol{s}^4$ and $\boldsymbol{z}'' = \boldsymbol{s}^3 - \boldsymbol{s}^4$. Inequality (21) implies

$$\begin{aligned} 0 &\le \mathcal{G}\left(\begin{pmatrix}\boldsymbol{y}'\\ \bar{\boldsymbol{y}}'\end{pmatrix},\begin{pmatrix}\boldsymbol{y}'\\ \bar{\boldsymbol{y}}'\end{pmatrix},\begin{pmatrix}\boldsymbol{z}''\\ \bar{\boldsymbol{z}}''\end{pmatrix},\begin{pmatrix}\boldsymbol{z}''\\ \bar{\boldsymbol{z}}''\end{pmatrix}\right) \\ &\quad + \mathcal{G}\left(\begin{pmatrix}\boldsymbol{y}''\\ \bar{\boldsymbol{y}}''\end{pmatrix},\begin{pmatrix}\boldsymbol{y}''\\ \bar{\boldsymbol{y}}''\end{pmatrix},\begin{pmatrix}\boldsymbol{z}'\\ \bar{\boldsymbol{z}}'\end{pmatrix},\begin{pmatrix}\boldsymbol{z}'\\ \bar{\boldsymbol{z}}'\end{pmatrix}\right) \\ &= 2\sum_{\substack{i=1,2\\ j=3,4}} \mathcal{G}\left(\begin{pmatrix}\boldsymbol{s}^i\\ \bar{\boldsymbol{s}}^i\end{pmatrix},\begin{pmatrix}\boldsymbol{s}^i\\ \bar{\boldsymbol{s}}^i\end{pmatrix},\begin{pmatrix}\boldsymbol{s}^j\\ \bar{\boldsymbol{s}}^j\end{pmatrix},\begin{pmatrix}\boldsymbol{s}^j\\ \bar{\boldsymbol{s}}^j\end{pmatrix}\right) \\ &\quad - 8\mathcal{G}\left(\begin{pmatrix}\boldsymbol{s}^1\\ \bar{\boldsymbol{s}}^1\end{pmatrix},\begin{pmatrix}\boldsymbol{s}^2\\ \bar{\boldsymbol{s}}^2\end{pmatrix},\begin{pmatrix}\boldsymbol{s}^3\\ \bar{\boldsymbol{s}}^3\end{pmatrix},\begin{pmatrix}\boldsymbol{s}^4\\ \bar{\boldsymbol{s}}^4\end{pmatrix}\right). \end{aligned} \tag{37}$$

Secondly, applying again inequality (21)

$$\begin{aligned} 0 &\le \mathcal{G}\left(\begin{pmatrix}\boldsymbol{s}^i+\boldsymbol{s}^j\\ \bar{\boldsymbol{s}}^i+\bar{\boldsymbol{s}}^j\end{pmatrix},\begin{pmatrix}\boldsymbol{s}^i+\boldsymbol{s}^j\\ \bar{\boldsymbol{s}}^i+\bar{\boldsymbol{s}}^j\end{pmatrix},\begin{pmatrix}\boldsymbol{s}^i-\boldsymbol{s}^j\\ \bar{\boldsymbol{s}}^i-\bar{\boldsymbol{s}}^j\end{pmatrix},\begin{pmatrix}\boldsymbol{s}^i-\boldsymbol{s}^j\\ \bar{\boldsymbol{s}}^i-\bar{\boldsymbol{s}}^j\end{pmatrix}\right) \\ &= \mathcal{G}\left(\begin{pmatrix}\boldsymbol{s}^i\\ \bar{\boldsymbol{s}}^i\end{pmatrix},\begin{pmatrix}\boldsymbol{s}^i\\ \bar{\boldsymbol{s}}^i\end{pmatrix},\begin{pmatrix}\boldsymbol{s}^i\\ \bar{\boldsymbol{s}}^i\end{pmatrix},\begin{pmatrix}\boldsymbol{s}^i\\ \bar{\boldsymbol{s}}^i\end{pmatrix}\right) \\ &\quad + \mathcal{G}\left(\begin{pmatrix}\boldsymbol{s}^j\\ \bar{\boldsymbol{s}}^j\end{pmatrix},\begin{pmatrix}\boldsymbol{s}^j\\ \bar{\boldsymbol{s}}^j\end{pmatrix},\begin{pmatrix}\boldsymbol{s}^j\\ \bar{\boldsymbol{s}}^j\end{pmatrix},\begin{pmatrix}\boldsymbol{s}^j\\ \bar{\boldsymbol{s}}^j\end{pmatrix}\right) \\ &\quad - 2\mathcal{G}\left(\begin{pmatrix}\boldsymbol{s}^i\\ \bar{\boldsymbol{s}}^i\end{pmatrix},\begin{pmatrix}\boldsymbol{s}^i\\ \bar{\boldsymbol{s}}^i\end{pmatrix},\begin{pmatrix}\boldsymbol{s}^j\\ \bar{\boldsymbol{s}}^j\end{pmatrix},\begin{pmatrix}\boldsymbol{s}^j\\ \bar{\boldsymbol{s}}^j\end{pmatrix}\right) \\ &\qquad\qquad \forall i=1,2 \quad j=3,4 \end{aligned} \tag{38}$$

Combining (37) and (38) yields

$$\begin{aligned} 8\mathcal{G}&\left(\begin{pmatrix}\boldsymbol{s}^1\\ \bar{\boldsymbol{s}}^1\end{pmatrix},\begin{pmatrix}\boldsymbol{s}^2\\ \bar{\boldsymbol{s}}^2\end{pmatrix},\begin{pmatrix}\boldsymbol{s}^3\\ \bar{\boldsymbol{s}}^3\end{pmatrix},\begin{pmatrix}\boldsymbol{s}^4\\ \bar{\boldsymbol{s}}^4\end{pmatrix}\right) \\ &\le 2\sum_{i=1}^{4}\mathcal{G}\left(\begin{pmatrix}\boldsymbol{s}^i\\ \bar{\boldsymbol{s}}^i\end{pmatrix},\begin{pmatrix}\boldsymbol{s}^i\\ \bar{\boldsymbol{s}}^i\end{pmatrix},\begin{pmatrix}\boldsymbol{s}^i\\ \bar{\boldsymbol{s}}^i\end{pmatrix},\begin{pmatrix}\boldsymbol{s}^i\\ \bar{\boldsymbol{s}}^i\end{pmatrix}\right) \end{aligned}$$

proving the desired inequality. ∎

D. Proof of Theorem 3.3

Proof: To study the convexity of a real valued function, recall the following theorem in convex analysis [31]:

Theorem A.2: Let us consider a real valued function $g : \mathbb{R}^n \to \mathbb{R}$, given $\boldsymbol{s}_0 \in \mathbb{R}^n$ and $\boldsymbol{h} \in \mathbb{R}^n$, define the restriction $\tilde{g}_{(\boldsymbol{s}_0,\boldsymbol{h})} : \mathbb{R} \to \mathbb{R}$ as $\tilde{g}_{(\boldsymbol{s}_0,\boldsymbol{h})}(t) = g(\boldsymbol{s}_0 + t\boldsymbol{h})$. Then, g is convex on $\mathbb{R}^n$ if and only if, for any $\boldsymbol{s}_0 \in \mathbb{R}^n$ and $\boldsymbol{h} \in \mathbb{R}^n$

- $\tilde{g}_{(\boldsymbol{s}_0,\boldsymbol{h})}(t)$ is convex on $\mathbb{R}$;
- $\tilde{g}''_{(\boldsymbol{s}_0,\boldsymbol{h})}(t) \ge 0$ for all $t \in \mathbb{R}$, assuming that the second order derivatives exist.

Notice that the value of $f(\boldsymbol{s})$ in (26) is always real, thus it can be viewed as real valued function with respect to the real variables $\Re(\boldsymbol{s})$ and $\Im(\boldsymbol{s})$. Let us now compute the second order derivatives associated with $f(\boldsymbol{s})$.

Lemma A.3: Assume that $f(\boldsymbol{s})$ is a complex quartic function; given $\boldsymbol{x},\boldsymbol{y} \in \mathbb{C}^N$, define $\tilde{f}_{(\boldsymbol{x},\boldsymbol{y})} : \mathbb{R} \to \mathbb{R}$ as $\tilde{f}_{(\boldsymbol{x},\boldsymbol{y})}(t) = f(\boldsymbol{x} + t\boldsymbol{y})$. Then, denoting by $\boldsymbol{z} = \boldsymbol{x} + t\boldsymbol{y}$, we have:

1) If $f(\boldsymbol{s}) = |\boldsymbol{s}^{\dagger}\boldsymbol{A}\boldsymbol{s}|^2$, then

$$\begin{aligned}\tilde{f}''_{(\boldsymbol{x},\boldsymbol{y})}(t) = 2\Big(&\boldsymbol{y}^{\dagger}\boldsymbol{A}\boldsymbol{y}\boldsymbol{z}^{\dagger}\boldsymbol{A}^{\dagger}\boldsymbol{z} + \boldsymbol{y}^{\dagger}\boldsymbol{A}\boldsymbol{z}\boldsymbol{y}^{\dagger}\boldsymbol{A}^{\dagger}\boldsymbol{z} + \boldsymbol{y}^{\dagger}\boldsymbol{A}\boldsymbol{z}\boldsymbol{z}^{\dagger}\boldsymbol{A}^{\dagger}\boldsymbol{y} \\ &+ \boldsymbol{z}^{\dagger}\boldsymbol{A}\boldsymbol{y}\boldsymbol{y}^{\dagger}\boldsymbol{A}^{\dagger}\boldsymbol{z} + \boldsymbol{z}^{\dagger}\boldsymbol{A}\boldsymbol{y}\boldsymbol{z}^{\dagger}\boldsymbol{A}^{\dagger}\boldsymbol{y} + \boldsymbol{z}^{\dagger}\boldsymbol{A}\boldsymbol{z}\boldsymbol{y}^{\dagger}\boldsymbol{A}^{\dagger}\boldsymbol{y}\Big)\end{aligned} \tag{39}$$

(40)

and it is always a real valued function.

2) If $\mathcal{H}$ is the conjugate-partial-symmetric fourth order tensor form such that $f(\boldsymbol{s}) = \mathcal{H}(\bar{\boldsymbol{s}},\boldsymbol{s},\bar{\boldsymbol{s}},\boldsymbol{s})$, then

$$\tilde{f}''_{(\boldsymbol{x},\boldsymbol{y})}(t) = 8\mathcal{H}(\bar{\boldsymbol{y}},\boldsymbol{y},\bar{\boldsymbol{z}},\boldsymbol{z}) + 2\mathcal{H}(\bar{\boldsymbol{y}},\boldsymbol{z},\bar{\boldsymbol{y}},\boldsymbol{z}) + 2\mathcal{H}(\bar{\boldsymbol{z}},\boldsymbol{y},\bar{\boldsymbol{z}},\boldsymbol{y})$$

and it is always a real valued function.

3) If $\mathcal{G}$ is the conjugate-super-symmetric fourth order tensor form such that $f(\boldsymbol{s}) = \mathcal{G}((\frac{\boldsymbol{s}}{\bar{\boldsymbol{s}}}),(\frac{\boldsymbol{s}}{\bar{\boldsymbol{s}}}),(\frac{\boldsymbol{s}}{\bar{\boldsymbol{s}}}),(\frac{\boldsymbol{s}}{\bar{\boldsymbol{s}}}))$, then

$$\tilde{f}''_{(\boldsymbol{x},\boldsymbol{y})}(t) = 12\mathcal{G}\left(\begin{pmatrix}\boldsymbol{y}\\ \bar{\boldsymbol{y}}\end{pmatrix},\begin{pmatrix}\boldsymbol{y}\\ \bar{\boldsymbol{y}}\end{pmatrix},\begin{pmatrix}\boldsymbol{z}\\ \bar{\boldsymbol{z}}\end{pmatrix},\begin{pmatrix}\boldsymbol{z}\\ \bar{\boldsymbol{z}}\end{pmatrix}\right)$$

and it is always a real valued function.

Proof: We only prove the statement (2); all the other situations are almost the same. In the considered case,

$$\tilde{f}_{(\boldsymbol{x},\boldsymbol{y})}(t) = \mathcal{H}(\overline{\boldsymbol{x}+t\boldsymbol{y}},\boldsymbol{x}+t\boldsymbol{y},\overline{\boldsymbol{x}+t\boldsymbol{y}},\boldsymbol{x}+t\boldsymbol{y}).$$

Due to the conjugate-partial-symmetry,

$$\begin{aligned}\tilde{f}'_{(\boldsymbol{x},\boldsymbol{y})}(t) = &\ 2\mathcal{H}(\bar{\boldsymbol{y}},\boldsymbol{x}+t\boldsymbol{y},\overline{\boldsymbol{x}+t\boldsymbol{y}},\boldsymbol{x}+t\boldsymbol{y}) \\ &+ 2\mathcal{H}(\overline{\boldsymbol{x}+t\boldsymbol{y}},\boldsymbol{y},\overline{\boldsymbol{x}+t\boldsymbol{y}},\boldsymbol{x}+t\boldsymbol{y})\end{aligned}$$

and

$$\begin{aligned}\tilde{f}''_{(\boldsymbol{x},\boldsymbol{y})}(t) &= 2\left(2\mathcal{H}(\overline{\boldsymbol{y}},\boldsymbol{y},\overline{\boldsymbol{x}+t\boldsymbol{y}},\boldsymbol{x}+t\boldsymbol{y})\right.\\ &\quad\left.+\mathcal{H}(\overline{\boldsymbol{y}},\boldsymbol{x}+t\boldsymbol{y},\overline{\boldsymbol{y}},\boldsymbol{x}+t\boldsymbol{y})\right)\\ &\quad+2\left(2\mathcal{H}(\overline{\boldsymbol{y}},\boldsymbol{y},\overline{\boldsymbol{x}+t\boldsymbol{y}},\boldsymbol{x}+t\boldsymbol{y})\right.\\ &\quad\left.+\mathcal{H}(\overline{\boldsymbol{x}+t\boldsymbol{y}},\boldsymbol{y},\overline{\boldsymbol{x}+t\boldsymbol{y}},\boldsymbol{y})\right)\\ &= 8\mathcal{H}(\overline{\boldsymbol{y}},\boldsymbol{y},\overline{\boldsymbol{x}+t\boldsymbol{y}},\boldsymbol{x}+t\boldsymbol{y})\\ &\quad+2\mathcal{H}(\overline{\boldsymbol{y}},\boldsymbol{x}+t\boldsymbol{y},\overline{\boldsymbol{y}},\boldsymbol{x}+t\boldsymbol{y})\\ &\quad+2\mathcal{H}(\overline{\boldsymbol{x}+t\boldsymbol{y}},\boldsymbol{y},\overline{\boldsymbol{x}+t\boldsymbol{y}},\boldsymbol{y}).\end{aligned}$$

Furthermore, exploiting Proposition A.1,

$$\begin{aligned}\mathcal{H}(\overline{\boldsymbol{y}},\boldsymbol{y},\overline{\boldsymbol{x}+t\boldsymbol{y}},\boldsymbol{x}+t\boldsymbol{y}) &= \bar{\mathcal{H}}(\boldsymbol{y},\overline{\boldsymbol{y}},\boldsymbol{x}+t\boldsymbol{y},\overline{\boldsymbol{x}+t\boldsymbol{y}})\\ &= \overline{\mathcal{H}(\overline{\boldsymbol{y}},\boldsymbol{y},\overline{\boldsymbol{x}+t\boldsymbol{y}},\boldsymbol{x}+t\boldsymbol{y})}\end{aligned}$$

and

$$\begin{aligned}\mathcal{H}(\overline{\boldsymbol{y}},\boldsymbol{x}+t\boldsymbol{y},\overline{\boldsymbol{y}},\boldsymbol{x}+t\boldsymbol{y}) &= \bar{\mathcal{H}}(\boldsymbol{x}+t\boldsymbol{y},\overline{\boldsymbol{y}},\boldsymbol{x}+t\boldsymbol{y},\overline{\boldsymbol{y}})\\ &= \overline{\mathcal{H}(\overline{\boldsymbol{x}+t\boldsymbol{y}},\boldsymbol{y},\overline{\boldsymbol{x}+t\boldsymbol{y}},\boldsymbol{y})}.\end{aligned}$$

Hence, as expected $\tilde{f}''_{(\boldsymbol{x},\boldsymbol{y})}(t)$ is always real. ■

Due to the arbitrariness of t and $\boldsymbol{y}$ in Lemma A.3, the vector $\boldsymbol{z}$, obtained through the variable transformation $\boldsymbol{x}+t\boldsymbol{y}\mapsto\boldsymbol{z}$, is a free complex variable with respect to $\boldsymbol{x}$. Thus, combining Lemma A.3 and Theorem A.2 we obtain the convexity characterization for the complex quartic function representations given in (19), (20), and (21). ■

E. Proof of Corollary 3.4

Proof: For a fixed λ, let $g(\boldsymbol{s})=\lambda(\boldsymbol{s}^\dagger\boldsymbol{s})^2-f(\boldsymbol{s})$. From Theorem 3.3, $g(\boldsymbol{s})$ is a convex function in $\boldsymbol{s}$ if and only if

$$\lambda\left(2\boldsymbol{y}^\dagger\boldsymbol{y}\boldsymbol{z}^\dagger\boldsymbol{z}+(\boldsymbol{y}^\dagger\boldsymbol{z}+\boldsymbol{z}^\dagger\boldsymbol{y})^2\right)-h(\boldsymbol{y},\boldsymbol{z})\geq 0,\quad\forall\boldsymbol{y},\boldsymbol{z}\in\mathbb{C}^N.$$

Furthermore, let us define

$$\lambda^*=\max_{\|\boldsymbol{z}\|=1,\|\boldsymbol{y}\|=1}h(\boldsymbol{y},\boldsymbol{z}),$$

which is a finite real number due to the compactness of the feasible set and the continuity of the function $h(\boldsymbol{y},\boldsymbol{z})$. Additionally, since $h(\boldsymbol{y},\boldsymbol{z})$ is a biquadratic function on $\boldsymbol{z}$ and $\boldsymbol{y}$,

$$\lambda^*\geq h\left(\frac{\boldsymbol{y}}{\|\boldsymbol{y}\|},\frac{\boldsymbol{z}}{\|\boldsymbol{z}\|}\right)=h(\boldsymbol{y},\boldsymbol{z})/\boldsymbol{y}^\dagger\boldsymbol{y}\boldsymbol{z}^\dagger\boldsymbol{z}\quad\forall\boldsymbol{y},\boldsymbol{z}\in\mathbb{C}^N.$$

Therefore for any $\lambda\geq\frac{1}{2}\lambda^*$,

$$\begin{aligned}&\lambda\left(2\boldsymbol{y}^\dagger\boldsymbol{y}\boldsymbol{z}^\dagger\boldsymbol{z}+(\boldsymbol{y}^\dagger\boldsymbol{z}+\boldsymbol{z}^\dagger\boldsymbol{y})^2\right)-h(\boldsymbol{y},\boldsymbol{z})\\ &\qquad\geq\lambda^*\left(\boldsymbol{y}^\dagger\boldsymbol{y}\boldsymbol{z}^\dagger\boldsymbol{z}\right)-h(\boldsymbol{y},\boldsymbol{z})\geq 0.\end{aligned}$$

Thus, condition (22) is satisfied and the conclusion follows. ■

F. Proof of Theorem 3.5

Proof: Applying (25) to $\boldsymbol{y}=\boldsymbol{y}_1-\boldsymbol{z}_1$ and $\boldsymbol{z}=\boldsymbol{y}_1+\boldsymbol{z}_1$,

$$\begin{aligned}0&\leq 2\mathcal{H}(\overline{\boldsymbol{y}_1+\boldsymbol{z}_1},\boldsymbol{y}_1+\boldsymbol{z}_1,\overline{\boldsymbol{y}_1-\boldsymbol{z}_1},\boldsymbol{y}_1-\boldsymbol{z}_1)\\ &\quad+\mathcal{H}(\overline{\boldsymbol{y}_1+\boldsymbol{z}_1},\boldsymbol{y}_1-\boldsymbol{z}_1,\overline{\boldsymbol{y}_1+\boldsymbol{z}_1},\boldsymbol{y}_1-\boldsymbol{z}_1)\\ &\quad+\mathcal{H}(\overline{\boldsymbol{y}_1-\boldsymbol{z}_1},\boldsymbol{y}_1+\boldsymbol{z}_1,\overline{\boldsymbol{y}_1-\boldsymbol{z}_1},\boldsymbol{y}_1+\boldsymbol{z}_1)\\ &=4\left(\mathcal{H}(\bar{\boldsymbol{y}}_1,\boldsymbol{y}_1,\bar{\boldsymbol{y}}_1,\boldsymbol{y}_1)+\mathcal{H}(\bar{\boldsymbol{z}}_1,\boldsymbol{z}_1,\bar{\boldsymbol{z}}_1,\boldsymbol{z}_1)\right)\\ &\quad-8\mathcal{H}(\bar{\boldsymbol{y}}_1,\boldsymbol{y}_1,\bar{\boldsymbol{z}}_1,\boldsymbol{z}_1),\end{aligned}$$

and the conclusion follows. ■

G. Local Convergence Analysis for Algorithm MBIL and Algorithm MBIQ

To address the local convergence analysis of the proposed procedures, let us associate to any vector $\boldsymbol{s}\in\Omega_\infty$ its phase vector $\boldsymbol{\phi}=[\phi(1),\phi(2),\ldots,\phi(N)]$, such that $\boldsymbol{s}=[e^{j\phi(1)},e^{j\phi(2)},\ldots,e^{j\phi(N)}]$.

- Let us focus on **Algorithm MBIL**. The optimization problem of interest is

$$\mathrm{P}_1^\infty\ \begin{cases}\max\limits_{\boldsymbol{s}^1,\boldsymbol{s}^2,\boldsymbol{s}^3,\boldsymbol{s}^4} & \mathcal{G}^\lambda\left(\begin{pmatrix}\boldsymbol{s}^1\\ \bar{\boldsymbol{s}}^1\end{pmatrix},\begin{pmatrix}\boldsymbol{s}^2\\ \bar{\boldsymbol{s}}^2\end{pmatrix},\begin{pmatrix}\boldsymbol{s}^3\\ \bar{\boldsymbol{s}}^3\end{pmatrix},\begin{pmatrix}\boldsymbol{s}^4\\ \bar{\boldsymbol{s}}^4\end{pmatrix}\right)\\ \text{s.t.} & \boldsymbol{s}^1,\boldsymbol{s}^2,\boldsymbol{s}^3,\boldsymbol{s}^4\in\Omega_\infty\end{cases}$$

Let us associate to $\boldsymbol{s}^i$, $i=1,2,3,4$ the phase vector $\boldsymbol{\phi}^i$, $i=1,2,3,4$, and let us denote by $\widehat{\mathcal{G}^\lambda}(\boldsymbol{\phi}^1,\boldsymbol{\phi}^2,\boldsymbol{\phi}^3,\boldsymbol{\phi}^4)$ the multi-block function such that

$$\widehat{\mathcal{G}^\lambda}(\boldsymbol{\phi}^1,\boldsymbol{\phi}^2,\boldsymbol{\phi}^3,\boldsymbol{\phi}^4)=\mathcal{G}^\lambda\left(\begin{pmatrix}\boldsymbol{s}^1\\ \bar{\boldsymbol{s}}^1\end{pmatrix},\begin{pmatrix}\boldsymbol{s}^2\\ \bar{\boldsymbol{s}}^2\end{pmatrix},\begin{pmatrix}\boldsymbol{s}^3\\ \bar{\boldsymbol{s}}^3\end{pmatrix},\begin{pmatrix}\boldsymbol{s}^4\\ \bar{\boldsymbol{s}}^4\end{pmatrix}\right).$$

Hence, the constrained optimization problem P_1^∞ is equivalent to the unconstrained problem

$$\widehat{\mathrm{P}}_1^\infty\ \left\{\max_{\boldsymbol{\phi}^1,\boldsymbol{\phi}^2,\boldsymbol{\phi}^3,\boldsymbol{\phi}^4}\ \widehat{\mathcal{G}^\lambda}(\boldsymbol{\phi}^1,\boldsymbol{\phi}^2,\boldsymbol{\phi}^3,\boldsymbol{\phi}^4)\right.\ .$$

Notice that in the k-th iteration of **Algorithm MBIL** applied to $\widehat{\mathrm{P}}_1^\infty$, we calculate $\phi_k^i(\ell)=-\arg(c^i(\ell))\in[0,2\pi[$ for $1\leq i\leq 4$ and $1\leq\ell\leq N$ (with $\boldsymbol{c}^i=(c^i(1),c^i(2),\ldots,c^i(N))$ defined as in footnote 6), and then update the block with the maximum improvement. Before proceeding further, let us define the energy norm associated with the matrix $\boldsymbol{A}\prec\boldsymbol{0}$, as

$$\|\boldsymbol{x}\|_{\boldsymbol{A}}=|\boldsymbol{x}^\dagger\boldsymbol{A}\boldsymbol{x}|^{\frac{1}{2}}.$$

Now by applying Theorem 3.1 in [41] we have the following result.

Theorem A.4: Let $\hat{\boldsymbol{\phi}}=(\hat{\boldsymbol{\phi}}^1,\hat{\boldsymbol{\phi}}^2,\hat{\boldsymbol{\phi}}^3,\hat{\boldsymbol{\phi}}^4)$ be a local maximum of problem $\widehat{\mathrm{P}}_1^\infty$ and $\{\boldsymbol{\phi}_k\}$ be the sequence generated by **Algorithm MBIL**, which converges to $\hat{\boldsymbol{\phi}}$. Supposing that $\boldsymbol{A}=\nabla^2\widehat{\mathcal{G}^\lambda}(\hat{\boldsymbol{\phi}})$ is negative definite, whenever the initial point $\boldsymbol{\phi}_0$ is close enough to $\hat{\boldsymbol{\phi}}$, the sequence $\{\boldsymbol{\phi}_k\}$ converges at least Q-linearly to $\hat{\boldsymbol{\phi}}$ in the energy norm, i.e., there exists $0\leq q\leq 1$ such that

$$\|\boldsymbol{\phi}_{k+1}-\hat{\boldsymbol{\phi}}\|_{\boldsymbol{A}}=q\,\|\boldsymbol{\phi}_k-\hat{\boldsymbol{\phi}}\|_{\boldsymbol{A}}.$$

- Let us focus on **Algorithm MBIQ**. The optimization problem of interest is

$$\mathrm{P}_2^\infty\ \begin{cases}\min\limits_{\boldsymbol{s}^1,\boldsymbol{s}^2} & \mathcal{H}^\lambda\left(\bar{\boldsymbol{s}}^1,\boldsymbol{s}^1,\bar{\boldsymbol{s}}^2,\boldsymbol{s}^2\right)\\ \text{s.t.} & \boldsymbol{s}^1,\boldsymbol{s}^2\in\Omega_\infty\end{cases}.$$

Like for **Algorithm MBIL**, we can construct the function $\widehat{\mathcal{H}^\lambda}(\boldsymbol{\phi}^1,\boldsymbol{\phi}^2)$ such that $\widehat{\mathcal{H}^\lambda}(\boldsymbol{\phi}^1,\boldsymbol{\phi}^2)=\mathcal{H}^\lambda(\bar{\boldsymbol{s}}^1,\boldsymbol{s}^1,\bar{\boldsymbol{s}}^2,\boldsymbol{s}^2)$. Thus, the constrained optimization problem $\mathrm{P}_2{}^\infty$ is equivalent to

$$\widehat{\mathrm{P}}_2^\infty\ \left\{\max_{\boldsymbol{\phi}^1,\boldsymbol{\phi}^2}\ \widehat{\mathcal{H}^\lambda}(\boldsymbol{\phi}^1,\boldsymbol{\phi}^2)\right.\ .$$

Applying Theorem 3.1 in [41], we have the following local linear convergence result for **Algorithm MBIQ**.

Theorem A.5: Let $\hat{\boldsymbol{\phi}} = (\hat{\boldsymbol{\phi}}^1, \hat{\boldsymbol{\phi}}^2)$ be a local maximum of problem $\widehat{\mathrm{P}}_2^{\infty}$ and $\{\boldsymbol{\phi}_k\}$ be the sequence generated by **Algorithm MBIQ**, which converges to $\hat{\boldsymbol{\phi}}$. Supposing that $\boldsymbol{A} = \nabla^2 \widehat{\mathcal{H}^{\lambda}}(\hat{\boldsymbol{\phi}})$ is negative definite and that $\boldsymbol{\phi}_k$ is obtained optimally solving the quadratic subproblems, whenever the starting point $\boldsymbol{\phi}_0$ is close enough to $\hat{\boldsymbol{\phi}}$, $\{\boldsymbol{\phi}_k\}$ is Q-linearly convergent to $\hat{\boldsymbol{\phi}}$.

ACKNOWLEDGMENT

The authors thank the Associate Editor Dr. M. Greco for carefully coordinating the revision of this paper and the anonymous Referees for the interesting and pertinent comments.

REFERENCES

[1] N. Levanon and E. Mozeson, *Radar Signals*. Hoboken, NJ, USA: Wiley, 2004.
[2] F. Gini, A. De Maio, and L. Patton, *Waveform Design and Diversity for Advanced Radar Systems*. London, U.K.: IET Radar and Sonar Navigation, 2011.
[3] D. E. Vakman, *Sophisticated Signals and the Uncertainty Principle in Radar*. Berlin, Germany: Springer-Verlag, 1968.
[4] S. M. Sussman, "Least-square synthesis of radar ambiguity functions," *IRE Trans. Inf. Theory*, vol. 8, no. 3, pp. 246–254, Apr. 1962.
[5] J. D. Wolf, G. M. Lee, and C. E. Suyo, "Radar waveform synthesis by mean-square optimization techniques," *IEEE Trans. Aerosp. Electron. Syst.*, vol. 5, no. 4, pp. 611–619, Jul. 1969.
[6] Y. I. Abramovich, B. G. Danilov, and A. N. Meleshkevich, "Application of integer programming to problems of ambiguity function optimization," *Radio Eng. Elect. Phys.*, vol. 22, no. 5, pp. 48–52, 1977.
[7] P. Stoica, H. He, and J. Li, "New algorithms for designing unimodular sequences with good correlation properties," *IEEE Trans. Signal Process.*, vol. 57, no. 4, pp. 1415–1425, Apr. 2009.
[8] M. Soltanalian and P. Stoica, "Computational design of sequences with good correlation properties," *IEEE Trans. Signal Process.*, vol. 60, no. 5, pp. 2180–2193, May 2012.
[9] H. Luke, "Sequences and arrays with perfect periodic correlation," *IEEE Trans. Aerosp. Electron. Syst.*, vol. 24, no. 3, pp. 287–294, May 1988.
[10] P. Stoica, H. He, and J. Li, "On designing sequences with impulse-like periodic correlation," *IEEE Trans. Signal Process. Lett.*, vol. 16, no. 8, pp. 703–706, Aug. 2009.
[11] J. J. Benedetto and J. J. Donatelli, "Ambiguity function and frame-theoretic properties of periodic zero-autocorrelation waveforms," *IEEE J. Sel. Topics Signal Process*, vol. 1, no. 1, pp. 6–20, Jun. 2007.
[12] J. R. Guerci, *Cognitive Radar, The Knowledge-Aided Fully Adaptive Approach*. : Artech House, 2010.
[13] T. Aittomaki and V. Koivunen, "Beampattern optimization by minimization of quartic polynomial," in *Proc. IEEE Statist. Signal Process. Workshop*, Cardiff, U.K., Aug. 2009, pp. 437–440.
[14] Z. Li, S. He, and S. Zhang, *Approximation Methods for Polynomial Optimization*. Berlin, Germany: Springer-Verlag, 2012.
[15] M. Laurent, "Sums of Squares, Moment Matrices and Optimization over Polynomials," in *Emerging Applications of Algebraic Geometry*, M. Putinar and S. Sullivant, Eds. Berlin, Germany: Springer-Verlag, 2009, pp. 157–270.
[16] S. Haykin, "Cognitive radar: A way of the future," *IEEE Signal Process. Mag.*, vol. 23, no. 1, pp. 30–40, Jan. 2006.
[17] A. De Maio, S. De Nicola, Y. Huang, Z.-Q. Luo, and S. Zhang, "Design of phase codes for radar performance optimization with a similarity constraint," *IEEE Trans. Signal Process.*, vol. 57, no. 2, pp. 30–40, Feb. 2009.
[18] M. Soltanalian and P. Stoica, "Designing unimodular codes via quadratic optimization is not always hard," *IEEE Trans. Signal Process.*, vol. 57, no. 6, Jun. 2009.
[19] B. Chen, S. He, Z. Li, and S. Zhang, "Maximum block improvement and polynomial optimization," *SIAM J. Optimiz.*, vol. 22, no. 11, pp. 87–107, Jan. 2012.
[20] A. Aubry, A. De Maio, A. Farina, and M. Wicks, "Knowledge-aided (potentially cognitive) transmit signal and receive filter design in signal-dependent clutter," *IEEE Trans. Aerosp. Electron. Syst.*, vol. 49, no. 1, pp. 93–117, Jan. 2013.
[21] National Land Cover Data (NLCD) [Online]. Available: http://landcover.usgs.gov, Available at
[22] C. T. Capraro, G. T. Capraro, A. De Maio, A. Farina, and M. Wicks, "Demonstration of knowledge-aided space-time adaptive processing using measured airborne data," *IEE Proc.-Radar Sonar Navig.*, vol. 153, no. 6, pp. 487–494, Dec. 2006.
[23] M. Skolnik, *Radar Handbook*, 3rd ed. New York, NY, USA: McGraw Hill, 2008.
[24] J. B. Billingsley, *Low-Angle Radar Land Clutter*. Raleigh, NC, USA: Scitech Publishing, 2002.
[25] M. Greco, F. Gini, A. Farina, and J. B. Billingsley, "Validation of wind-blown radar ground clutter spectral shape," *IEEE Trans. Aerosp. Electron. Syst.*, vol. 37, no. 2, pp. 538–548, Apr. 2001.
[26] B. Chen, "Optimization With Block Variables: Theory and Applications," Ph.D. dissertation, The Chinese Univesrity of Hong Kong, , Jun. 2012.
[27] S. Zhang and Y. Huang, "Complex quadratic optimization and semidefinite programming," *SIAM Jo. Optimiz.*, vol. 16, no. 3, pp. 871–890, Aug. 2006.
[28] B. Jang, Approximation Algorithms for Complex Homogeneous Polynomial Optimization Problems The Chinese Univ. Hong Kong, Progess Report, Nov. 2010.
[29] T. G. Kolda and B. W. Bader, "Tensor decompositions and applications," *SIAM Rev.*, vol. 51, no. 3, pp. 455–500, 2009.
[30] L. Qi, The Spectral Theory of Tensor (Rough Version) [Online]. Available: http://arxiv.org/pdf/1201.3424.pdf
[31] S. Boyd and L. Vandenberghe, *Convex Optimization*. Cambridge, U.K.: Cambridge Univ. Press, 2004.
[32] M. A. Richards, J. A. Scheer, and W. A. Holm, *Principles of Modern Radar: Basic Principles*. Raleigh, NC, USA: Scitech Publishing, 2010.
[33] A. Aubry, A. De Maio, M. Piezzo, A. Farina, and M. Wicks, "Cognitive Design of the Receive Filter and Transmitted Phase Code in Reverberating Environment," *IET Radar, Sonar Navigation*, vol. 6, no. 9, pp. 822–833, Dec. 2012.
[34] D. F. Delong, Jr. and E. M. Hofstetter, "The design of clutter-resistant radar waveforms with limited dynamic range," *IEEE Trans. Inf. Theory*, vol. IT-15, no. 3, pp. 376–385, May 1969.
[35] J. S. Thompson and E. L. Titlebaum, "The design of optimal radar waveforms for clutter rejection using the maximum principle," *IEEE Trans. Aerosp. Electron. Syst.*, vol. AES-3, pp. 581–589, Nov. 1967.
[36] A. I. Cohen, "An algorithm for designing burst waveforms with quantized transmitter weights," *IEEE Trans. Aerosp. Electron. Syst.*, vol. AES-11, no. 1, pp. 56–64, Jan. 1975.
[37] Y. I. Abramovich and M. B. Sverdlik, "Synthesis of filters maximizing the signal-to-noise ratio in the case of a minimax constraint on the sidelobes of the cross-ambiguity function," *Radio Eng. Electron. Phys.*, vol. 16, no. 11, pp. 253–258, Feb. 1971.
[38] P. Stoica, J. Li, and M. Xue, "On binary probing signals and instrumental variables receivers for radar," *IEEE Trans. Inf. Theory*, vol. 54, no. 8, pp. 3820–3825, Aug. 2008.
[39] Y. I. Abramovich and M. B. Sverdlik, "Synthesis of a filter which maximizes the signal-to-noise ratio under additional quadratic constraints," *Radio Eng. Electron. Phys.*, vol. 15, no. 11, pp. 1977–1984, Nov. 1970.
[40] J. Li, J. R. Guerci, and L. Xu, "Signal waveform's optimal-under-restriction design for active sensing," *IEEE Signal Process. Lett.*, vol. 13, no. 9, pp. 565–568, Sept. 2006.
[41] Z. Li, A. Uschmajew, and S. Zhang, Linear Convergence Analysis of the Maximum Block Improvement Method for Spherically Constrained Optimization Tech. Rep., 2013.

Augusto Aubry (M'12), photograph and biography not available at the time of publication.

Antonio De Maio (S'01–A'02–M'03–SM'07–F'13), photograph and biography not available at the time of publication.

Bo Jiang, photograph and biography not available at the time of publication.

Shuzhong Zhang, photograph and biography not available at the time of publication.